51/1-13-93 JS (2)

PREPARED FOR THE U.S. DEPARTMENT OF ENERGY,
UNDER CONTRACT DE-AC02-76-CHO-3073

PPPL-2859

PPPL-2859
UC-426

HIGH-RESOLUTION MEASUREMENTS, LINE IDENTIFICATION, AND SPECTRAL MODELING OF Kα TRANSITIONS IN Fe XVIII-XXV

BY

P. BEIERSDORFER, T. PHILLIPS, V.L. JACOBS, K.W. HILL, ET AL.

NOVEMBER, 1992

PPPL PRINCETON PLASMA PHYSICS LABORATORY

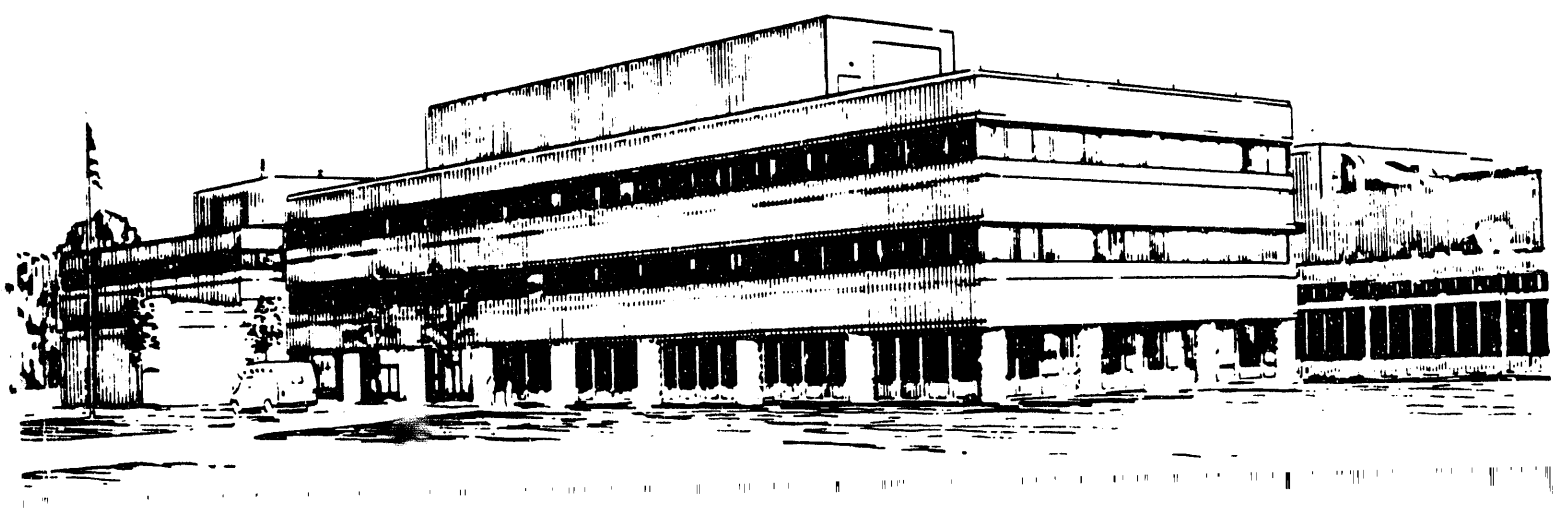

NOTICE

This report was prepared as an account of work sponsored by an agency of the United States Government. Neither the United States Government nor any agency thereof, nor any of their employees, makes any warranty, express or implied, or assumes any legal liability or responsibility for the accuracy, completeness, or usefulness of any information, apparatus, product, or process disclosed, or represents that its use would not infringe privately owned rights. Reference herein to any specific commercial produce, process, or service by trade name, trademark, manufacturer, or otherwise, does not necessarily constitute or imply its endorsement, recommendation, or favoring by the United States Government or any agency thereof. The views and opinions of authors expressed herein do not necessarily state or reflect those of the United States Government or any agency thereof.

NOTICE

This report has been reproduced from the best available copy.
Available in paper copy and microfiche.

Number of pages in this report:

DOE and DOE contractors can obtain copies of this report from:

Office of Scientific and Technical Information
P.O. Box 62
Oak Ridge, TN 37831;
(615) 576-8401.

This report is publicly available from the:

National Technical Information Service
Department of Commerce
5285 Port Royal Road
Springfield, Virginia 22161
(703) 487-4650

High-Resolution Measurements, Line Identification, and Spectral Modeling of Kα Transitions in Fe XVIII– XXV

P. Beiersdorfer and T. Phillips

University of California
Lawrence Livermore National Laboratory
Livermore, CA 94550

PPPL--2859

DE93 005723

V. L. Jacobs

Naval Research Laboratory
Condensed Matter and Radiation Sciences Division
Code 4694, Washington, DC 20375

K. W. Hill, M. Bitter, and S. von Goeler

Princeton University
Princeton Plasma Physics Laboratory, Princeton, NJ 08543

S. M. Kahn

University of California
Department of Physics and Astronomy and Space
Sciences Laboratory, Berkeley, CA 94720

Abstract

A detailed analysis of the iron Kα emission spectrum covering the wavelength region from 1.840 Å to 1.940 Å is presented. Measurements are made with a high-resolution Bragg crystal spectrometer on the Princeton Large Torus (PLT) tokamak for plasma conditions which closely resemble those of solar flares. A total of 40 features are identified consisting of either single or multiple lines from eight charge states in iron, Fe XVIII through Fe XXV, and their wavelengths are determined with an accuracy of 0.1–0.4 mÅ. Many of these features are identified for the first time. In the interpretation of our observations we rely on model calculations that determine the ionic species abundances from electron density and temperature profiles measured independently with non spectroscopic techniques and that incorporate theoretical collisional excitation and dielectronic recombination rates resulting in the excitation of the $1s2s^r2p^s$ configurations. The model calculations also include the effect of diffusive ion transport. Good overall agreement between the model calculations and the observations is obtained, which gives us confidence in our line identifications and spectral modeling capabilities. The results are compared with earlier analyses of the Kα emission from the Sun. While many similarities are found, a few differences arise from the somewhat higher electron density in tokamak plasmas (10^{13} cm^{-3}), which affects the fine-structure level populations of the ground states of the initial ion undergoing electron-impact excitation or dielectronic recombination. We also find that several spectral features are comprised of different transitions from those reported in earlier analyses of solar data.

MASTER

I. Introduction

Iron is the most abundant and, therefore, the most important high-Z element for the diagnostics of hot astrophysical plasmas. X-ray emission from the iron K shell has been observed in spectra of nearly all classes of cosmic x-ray sources, including active stellar coronae (e.g., White *et al.* 1986; Tsuru *et al.* 1989), compact x-ray binaries (e.g., White, Peacock, and Taylor 1985), supernova remnants (e.g., Tsunemi *et al.* 1986), clusters of galaxies (e.g., Mitchell *et al.* 1976; Serlemitsos *et al.* 1977; Ulmer *et al.* 1987), and active galactic nuclei (see review by Fabian and George, 1991). Scheduled x-ray missions such as ASTRO D, the Advanced X-Ray Astrophysics Facility (AXAF), and the X-Ray Multi-Mirror Mission (XMM) will provide considerable improvements in both, sensitivity and spectral resolution for iron K line detection. Iron is also an important element for the diagnostics of hot laboratory plasmas, especially those produced in magnetic-confinement fusion research, and its K-shell emission has been utilized extensively in the diagnostics of tokamak plasmas (Hill *et al.* 1979; Bitter *et al.* 1979a). The iron K-shell spectrum has been observed from a variety of other laboratory sources as well, such as vacuum sparks (Lie and Elton 1971), beam-foil interactions (Briand 1982), and, most recently, ion traps (Brown *et al.* 1989; Beiersdorfer 1990; Beiersdorfer *et al.* 1992a,c,d).

Eight different charge states, Fe XVIII through Fe XXV, contibute to the Kα emission in the wavelength range 1.85–1.93 Å. As a result, Kα emission data allow the detailed determination of equilibrium and nonequilibrium charge-state distributions and comparisons with charge-balance calculations. Iron K-shell data also provide measurements of the electron and ion temperatures, allow detection of non-Maxwellian electron distributions, and enable the deduction of plasma motion.

Because of the importance of the iron K-shell emission for diagnostics, exact line identification is crucial for proper analysis of spectral data. Among the astrophysical measurements, solar observations presently provide the highest-resolution iron K-shell x-ray data. The spectral resolution of these data typically lies between $\lambda/\Delta\lambda$= 1000–2500. This is more than sufficient to resolve dielectronic satellite and associated resonance lines and to utilize the data to infer plasma parameters. Identification and wavelengths of transitions in Fe XIX–XXV observed in solar flare spectra have been reported by various authors (Grineva *et al.* 1973; Korneev *et al.* 1979; Feldman, Doschek, and Kreplin 1980; Doschek, Feldman, and Cowan 1981). A most recent analysis of high-resolution iron K-shell data from solar flare observations was presented by Seely, Feldman, and Safronova (1986), in the following referred to as SFS, who identified transitions in all eight charge states Fe XVIII through Fe

XXV.

Precise wavelength data from laboratory sources are only available for K-shell transitions in Fe XXIII, Fe XXIV, and Fe XXV and have been derived from analyses of tokamak and beam-foil spectra (Bitter *et al.* 1979b; Briand *et al.* 1983; Bitter *et al.* 1988). No laboratory measurements that have similar precision as the solar flare measurements of SFS have been reported for transitions in Fe XVIII through Fe XXII. Such measurements are needed to compare with the solar results.

In the following we report measurements of iron K-shell transitions from high-resolution observations on the Princeton Large Torus (PLT) tokamak. The measurements were performed with improved spectral resolving power ($\lambda/\Delta\lambda = 3000$) and better counting statistics than past solar observations. We identified transitions in all eight charge states Fe XVIII through Fe XXV and determined their wavelengths within an accuracy of 0.1 – 0.4 mÅ. Many of the transitions that we observed in Fe XVIII through Fe XXII have not yet been identified in solar spectra and are identified here for the first time. We also point out several features which we determined to be comprised of transitions that are different from those reported in earlier analyses.

In interpreting our observations we rely heavily on model calculations that determine the ionic species abundances from measured electron density and temperature profiles, including the effects of ion diffusion, and that incorporate theoretical values of collisional excitation and dielectronic recombination rates computed by Jacobs *et al.* (1989) to predict the line intensities of Fe XVIII through Fe XXIV. The rates of Jacobs *et al.* (1989) were computed using separate simplifications assumed valid in three different electron density regimes: a collisionless, low-density regime ($\leq 10^{12}$ cm^{-3}) believed applicable for astrophysical plasmas such as solar flares, supernova remnants, and intercluster media; an intermediate-density regime (10^{13}–10^{14} cm^{-3}) for magnetically confined laboratory plasmas such as tokamaks and possibly for accretion-powered astrophysical sources; and a high-density regime ($\geq 10^{20}$ cm^{-3}) believed valid for laser-produced plasmas. The differences in the three regimes are due to collisional effects which determine the assumed initial population distribution among the fine-structure levels of the ground state of each ionic species. By using the rates of Jacobs *et al.* to identify features in our tokamak spectra, we are able to test their validity in the intermediate-density regime. We have found good overall agreement between calculated and observed intensities. The good overall agreement also validates the assumptions that enter into our charge balance calculation and intimates the utility of our model calculations for determining ion transport parameters.

Obvious disagreements between model intensities and measurements are found only for

a few features attributed to transitions in the lower charge states, such as Fe XIX and Fe XX. The disagreement appears to be a consequence of the strong dependence of the line emission on the electron density not adequately taken into account by the simplifications entering the calculations of the excitation rates. In some cases we find that the oberved line intensities fall in between the intensities predicted from the rates of Jacobs *et al.* (1989) in the low-density or intermediate-density approximation. Additional disagreement arises from inaccuracies in the theoretical wavelengths employed in our model. Because many lines overlap and blend, small changes in the assumed wavelengths result in very differently shaped emission features. We stress this point because this illustrates the need for highly accurate wavelength data; without accurate data features consisting of unresolved lines cannot be reliably predicted and observations cannot be properly interpreted.

The remainder of this paper is organized as follows. In Sec. II we discuss the plasma conditions that prevailed when our measurements were made on the PLT tokamak. Typical emission data are presented in Sec. III. The intensity modeling calculations are described in Sec. IV, whereby emphasis is placed on a discussion of the sensitivity of the resulting synthetic spectra to the theoretical ionization balance and to the assumed line positions. In Sec. V we present synthetic spectra for comparison with the experimental results followed by a detailed discussion of the identification of individual features in our spectra. This discussion is organized by wavelength region instead of ionization state. Here we point out similarities and differences between our tokamak data and solar flare measurements. Concluding remarks are presented in Sec. VI.

II. Plasma Conditions

The plasma conditions in tokamaks are the closest of any laboratory plasma to those encountered in many hot astrophysical x-ray sources. Peak electron temperatures in tokamaks typically range around several thousand electron-volts; peak electron densities range from 10^{12} to 10^{14} cm^{-3}. The parameters of tokamak plasmas are thus comparable to conditions encountered in solar flares and coronal plasmas of other active stars.

Tokamak plasmas are well diagnosed. Most importantly, plasma parameters relevant for atomic physics are determined with independent, non spectroscopic techniques such as laser scattering, microwave interferometry, electron cyclotron emission, and analysis of the continuous x-ray emission from bremsstrahlung. A review of the techniques is given by Orlinskij and Magyar (1988). As a result, tokamak plasmas are well suited to test atomic physics models in a controlled environment (Beiersdorfer *et al.* 1989c). Iron is an

indigenous impurity in PLT plasmas (von Goeler 1979), and radiation from various ion species can be observed under any plasma condition without prearrangement. Indeed, since the inception of the technique by Bitter *et al.* (1979a), high-resolution measurements of the K-shell emission from Fe XXV have served as the standard diagnostic on PLT to determine the ion temperature from the width of the resonance line.

Data presented in this paper are from relatively low-density, cool, ohmically heated discharges. Two typical electron temperature profiles are shown in Fig. 1(a). In the first profile (dashed curve) a peak temperature of 1.0 keV is attained. The peak temperature in the second profile (solid curve) is about 1.6 keV. In the following we shall refer to these two profiles as the "cold" and the "hot" cases. The electron density profiles are virtually identical for the hot and cold cases. A profile measured with laser scattering is shown in Fig. 1(b). The central electron density is 1.7×10^{13} cm^{-3}; the corresponding density averaged along a line of sight through the center of the plasma is 1×10^{13} cm^{-3}. The ion temperature is less than 1.0 keV; consequently, the broadening of a given x-ray line in iron due to the Doppler effect is less than $\Delta\lambda/\lambda < 1 : 3600$.

Figure 1 shows that the electron temperature varies from more than 1 keV in the center to a few eV at the edge of the plasma. As a result, the plasma contains radial shells of ions whose charge states are decreasing from the inside toward the edge. This effect is illustrated in Fig. 2. The figure shows the charge state distribution of iron ions for the hot electron temperature case of Fig. 1, calculated with the MIST code developed by Hulse (1983). This code uses the ionization and recombination rates of Post *et al.* (1977). A multiplier of 1.4 has been applied to all ionization rates in order to achieve agreement between charge distributions in coronal equilibrium calculated with the MIST code and those calculated by Jacobs *et al.* (1989), as discussed in Sec. IV. Because of the gradients in electron temperature and density, the charge state distribution is affected by radial transport of ions into hotter and colder regions. In calculating the radial charge distribution, we take into account transport of ions from hot to cold plasma regions and vice versa. In doing so, we assume that the ion transport is purely diffusive, i.e., we make the assumption that convective flows are absent, and we set the diffusion coefficient D=3000 cm^2/s. These assumptions are in accordance with a measurement by Beiersdorfer *et al.* (1989a) on the PLT tokamak, which determined D=5000 cm^2/s from radial profiles of the L-shell line emission of neonlike selenium for plasma conditions similar to those in the present investigation. The use of a different diffusion coefficient alters the calculated charge balance, but it does not change the conclusions drawn from the analysis presented in subsequent sections. On the contrary, the good agreement achieved between model calculations and measurements, which is presented

in subsequent sections, can be regarded as a validation of our assumption about tokamak plasma transport. Details of ionization balance calculations in tokamaks and the MIST code are given by Hulse (1983).

III. Spectral Observations

The iron Kα spectra are recorded with the Johann-type crystal spectrometer described by Hill *et al.* (1979). The spectrometer views the plasma along a sightline in the horizontal midplane of PLT as shown in Fig. 3. It was used earlier by Bitter *et al.* to measure the $1s2l2l'$ dielectronic satellite lines of Fe XXV (1979b) as well as to determine the contributions to the heliumlike resonance line from unresolved satellites of the type $1s2lnl'$ with $n \geq 3$ (1981).

For the present experiment the spectrometer was set up to record the iron Kα line emission from all eight charge states Fe XVIII through Fe XXV in the wavelength region between 1.85 Å and 1.95 Å in a single setting. For this purpose the spectrometer employs a 6-in.×1.5-in.×0.03-in. quartz crystal cut parallel to the $11\bar{2}0$ plane and bent to a radius of curvature of 276 cm. The $2d_{\infty}$ spacing of this crystal plane equals 4.913 Å at 25° C (Wyckoff 1963). Measurements are made in second order Bragg reflection at a Bragg angle of about 50° to insure good spectral resolution. A multiwire proportional counter with a sensitive area of 10×18 cm^2 is employed to record the spectra. The counter is filled with a mixture of 90% krypton and 10% carbon dioxide. This gas mixture results in a constant detection efficiency over the observed range of photon energies. Adjustable lead apertures are placed in front of the crystal in order to limit the count rate to $< 5 \times 10^5$ photons/sec. In our experiment, the illuminated length of the crystal was 9 cm. The resolving power $\lambda/\Delta\lambda$ of the instrument is about 3000, which is comparable to the Doppler-broadened line width.

Two iron Kα emission spectra observed under the conditions corresponding to the cold and hot electron temperature profiles of Fig. 1 are presented in Figs. 4(a) and 5(a), respectively. Here spectral features are labeled by the ionic species that contributes most to the emission. An exception is made for the well studied heliumlike transitions in Fe XXV, which are labeled in the notation of Gabriel (1972) as w, x, y, and z (cf. Table I). Because of the differences in electron temperature, the charge distribution is very different in the two cases. As a result, the spectral line emission is very different, giving rise to spectra that differ drastically from each other. In the following we use these two spectra as benchmarks to test our intensity model and for line identification.

IV. Intensity Modeling

Transitions in berylliumlike Fe XXIII through heliumlike Fe XXV have been studied extensively in the laboratory, and their identities are well established. This is not the case for transitions in the lower ionization stages Fe XVIII (fluorinelike) through Fe XXI (boronlike), whose emission often is much weaker. Comparing spectra that are produced in a hot plasma with those from a cold plasma (cf. Figs. 4 and 5) provides useful information for identifying which ionic species is emitting a given set of lines. However, identification of individual lines is difficult for those ionic species with partially filled subshells, as a multitude of transitions from the same as well as from different ionic species intertwine and blend. Transitions can be excited by both dielectronic capture and electron-impact excitation, and the observation of a given line may depend on the electron density, as electron collisions populate and depopulate the various fine structure levels of the ionic ground states (Mason *et al.* 1979; Phillips *et al.* 1983; Lemen *et al.* 1986). As a consequence, line identification can not solely rely on wavelength data or oscillator strengths from atomic structure codes, but must take into account information on the excitation mechanisms and predicted intensity of each possible transition.

In order to carry out the interpretation of the observed spectral features we have constructed a model that predicts the relative intensities of iron K-shell transitions from the charge balance, electron-impact excitation rates, and dielectronic recombination rates, given a measured temperature and density profile. In the model, the emissivity ϵ of a given line j from an ion with charge q is expressed by

$$\epsilon_j = \int [n_q C_j + n_{q+1} \alpha_j] n_e dr. \tag{1}$$

Here C_j is the rate coefficient for excitation by electron collisions, and α_j is the rate coefficient for dielectronic recombination that populates the upper level of transition j; n_e is the measured electron density. Rates have been calculated by Jacobs *et al.* (1989) and take into account the population distribution among the fine structure levels of the respective ground states of species q and $q+1$. The species abundances n_q and n_{q+1} are obtained from ionization-balance calculations employing the MIST code (Hulse 1983) described above. Note that the measured electron temperature enters in the calculation of both the rate coefficients and the ionic species abundance. The integration is performed along the sightline of the spectrometer, i.e., along a line of sight through the center of the plasma. No line excitation mechanisms other than electron-impact excitation and dielectronic recombination are included in the model, and among these only those processes are included that

produce excited electrons in the n=2 shell. Dielectronic capture processes into the n=3 shell, for example, which strongly contribute to the feature on the long-wavelength side of the heliumlike resonance line w (Bely-Dubau, Gabriel, and Volonté 1979; Bitter *et al.* 1981), are not considered. Furthermore, emissivities are calculated only for transitions in Fe XVIII through Fe XXIV, i.e., no calculations are made for those of the heliumlike lines w, x, y, and z. The intensities of the heliumlike lines have been the subjects of an ongoing debate, and even very sophisticated models do not describe their intensities adequately if the electron temperature is low (Bitter *et al.* 1985; Doschek 1990; Bitter *et al.* 1991).

Before we apply our model calculations to the analysis of experimental spectra, two important theoretical parameters must be checked. These are the ionization and recombination rates, which determine the theoretical ionization balance, and the calculated line positions. Adequate knowledge of the latter is especially important for lines that blend.

In a first check, we calculate synthetic spectra in the coronal equilibrium limit, assuming a constant electron temperature of 862 eV throughout the plasma. This allows us to compare our results to the synthetic spectra calculated by Jacobs *et al.* (1989). Results of our calculations are shown in Fig. 6. The spectrum in Fig. 6(a) is calculated using the ionization and recombination rates of Post *et al.* (1977), which are the default values in the MIST code. These produce a charge balance lower than that calculated by Jacobs *et al.* (1989). To match the calculations by Jacobs, the ionization rates of all species were increased by 40%. The corresponding spectrum is shown in Fig. 6(b). A comparison of the two spectra in (a) and (b) demonstrates the sensitivity of the synthetic spectra to the exact values of the ionization and recombination rates and thus to the charge balance. In subsequent calculations we use ionization rates that are 1.4 times larger than the default values, not only because they yield a charge balance in agreement with that of Jacobs *et al.* (1989) but also because they provide synthetic spectra that are better matches to the experimental data.

The synthetic emission spectra in Figs. 6(a) and (b) are calculated using theoretical line positions provided by Jacobs *et al.* (1989). These line positions were calculated with the relativistic multiconfiguration code developed by Cowan (1981) and have been estimated to be accurate within 2–3 mÅ (Jacobs *et al.* 1989). In Fig. 6(c) we have recalculated the emission spectrum of Fig. 6(b) using the semiempirical wavelengths reported by SFS, augmented and modified based on our own set of wavelength calculations described below. The SFS line positions were calculated with the Z-expansion technique and for each ionization state were shifted by a common value to give best overall agreement with the solar iron K-shell observations. The SFS values were estimated to be accurate within 0.25–0.65 mÅ, and they indeed provide a close match with our experimental values.

Because our synthetic spectra comprise more transitions than calculated by SFS, we have augmented their list with several transitions whose line positions we have estimated from our own calculations. For this, we performed energy level calculations for Fe XVIII through Fe XXIII using the relativistic atomic structure code RAC developed by Scofield (1991). The RAC code performs multi-configurational structure calculations similar to the extended average level calculations of the GRASP code described by Grant *et al.* (1980). The wavelengths calculated with RAC are estimated to be less accurate than those provided by SFS. Values calculated with RAC are listed together with the SFS values in Tables I through VI, and the two calculations differ on the average by as little as 0.6 mÅ for Fe XXIII and Fe XXII and as much as 1.6 mÅ for Fe XIX. Because the difference between the two calculations is, to first approximation, the same for each transition within a given ionization state, we can estimate the line positions of lines not tabulated by SFS and complete the list of wavelengths used for generating the synthetic spectrum in Fig. 6(c). Line positions inferred in this way are listed in Tables I through IV among the SFS values and are identified as "estimates."

We shifted the positions of some of the lines in Fe XX and Fe XIX by a small amount (typically less than 0.5 mÅ) from the SFS values. This shift provides better agreement between the synthetic spectra and observations. We also shifted several individual lines by somewhat larger amounts. These include lines $N11$, $N14$, $O9$, and $F1$. Our model predicts these lines to be relatively intense, yet in the wrong position when compared to the experimental data. In many cases, this shift is justified by estimating relative line positions from our RAC calculations. For example, the RAC prediction for the $1s2s^22p^5\ {}^2P_{3/2}$ — $1s^22s^22p^5\ {}^2S_{1/2}$ transition in Fe XVIII differs considerably from that given by SFS. They predicted its wavelength to be 1.9215 Å. By contrast, the RAC calculation predicts a value of 1.9254 Å, which is 3.9 mÅ higher. Because the RAC value for the second, ${}^2P_{1/2} - {}^2S_{1/2}$ transition in Fe XVIII is 2.15 mÅ *less* than the value given by SFS, we estimate the position of the line to be at 1.92755 Å and use this value in generating the synthetic spectra (cf. Table VI). This is discussed in detail below. The line positions of transitions in Fe XX and Fe XIX that we have adopted for generating subsequent sythetic spectra are listed separately from the SFS values in Tables V and VI.

A comparison of the spectra in Figs. 6(b) and (c) demonstrates the sensitivity of synthetic emission spectra to the exact values of the line positions. Transitions from a given ionic species do not simply shift positions in unison but change positions relative to each other. Although the shift relative to each other is much smaller than the overall shift, it has a pronounced effect on the shape of the predicted emission features. This sensitivity is

most pronounced when several lines blend, and the overall shape of a blend of lines changes drastically as different individual line positions are assumed. Because we use the synthetic spectra to identify individual transitions in the observed spectra, it is thus imperative to use the most accurate available structure data in generating model spectra.

V. Line Identification and Wavelength Determination

Adopting the ionization rates and line positions employed to generate the spectrum in Fig. 6(c), we use our intensity model to generate synthetic spectra for comparison with the two experimental spectra of Figs. 4(a) and 5(a). The resulting synthetic spectra are shown as subfigures 4(b) and 5(b). The calculated relative line intensities for both, the hot and cold case are listed in Tables I through VI for all lines whose relative intensity is 0.01 or larger.

Good overall agreement between synthetic and experimental emission spectra can be noted by comparing subfigures (a) and (b) in 4 and 5. The calculated line intensities match the observed intensities remarkably well. Because of this agreement we feel confident in using the synthetic spectra for line identification. A list of our identifications is given in Tables I through VI. An overview of our identifications is also given in Fig. 7, where we have marked features using the key of Tables I through VI. A given feature consisting of several lines is labeled by all lines that contribute at least 20% to its intensity. A line contributing more than 50% of the total is underlined.

The good overall agreement of the synthetic spectra with the observations is somewhat surprising considering the neglect of many excitation processes that can affect the line emission, such as innershell ionization, radiative cascades from levels higher than n=2, charge-transfer processes, and radiative recombination. A disagreement, for example, is found in the set of lines due to oxygenlike Fe XIX between 1.910 Å and 1.920 Å. The observations in Fig. 4(a) show one intense feature at 1.917 Å preceeded by two weaker features. The calculations presented in Fig. 4(b), on the other hand, predict this line to be weaker and preceded by a more intense line, i.e., the line labeled $O3$ in Table VI. Despite this disagreement, however, there is sufficient agreement between the sythetic spectra and observations to allow a reasonable match between the transitions that produce the features.

The emission from Fe XXII, Fe XXI, Fe XX, and Fe XIX depends strongly on the value of the electron density (Mason *et al.* 1979; Phillips *et al.* 1983; Lemen *et al.* 1986; Jacobs *et al.* 1989) because their ground-state configurations have multiple fine-structure levels whose relative populations are sensitive to the effects of collisional processes. This suggests

that some discrepancies between the intensities of features in our sythentic spectra and observations might be due to density effects. Our model calculations assume ground level populations presumed valid for the intermediate-density regime $10^{13} - 10^{14}$ cm^{-3}. The electron density in tokamak plasmas, however, is a spatially varying quantity, and is lower at the edge than in the center, as demonstrated by the profile in Fig. 1. It is conceivable that some of the line emission, especially from ions in low ionization stages, emanates from low-density regions where the ground-state population distributions assumed in the intermediate-density limit are not valid. Consequently, we recalculated the iron emission spectra using excitation rates in the low-density approximation of Jacobs *et al.* (1989). The results of these calculations are shown in subfigures 4(c) and 5(c). The intensities of the lower ionic species differ drastically from those obtained in the intermediate-density limit and do not match the observations. Although some discrepancies between our synthetic spectra and observations may indeed be caused by density effects, as discussed in more detail below, we conclude that the intermediate-density approximation produces synthetic spectra that are much more closely matched to the observations than the spectra obtained in the low-density limit.

A. Wavelength Determinations

The wavelength λ of a given line is determined by Bragg's law (Compton and Allison 1935)

$$n\lambda = 2d_n \sin\theta \quad , \tag{2}$$

where n is the order of diffraction and θ is the Bragg angle. The value of d_n can be calculated from the expression

$$d_n = d_\infty(1 - (2d_\infty)^2\delta/n^2\lambda^2) \quad , \tag{3}$$

where δ is the deviation of the index of refraction from unity. Following Compton and Allison (1935), the value of δ/λ^2 is assumed to be independent of wavelength and equal to 3.64×10^{-6} Å^{-2} for quartz. The Bragg angle θ of a line whose center position is observed in channel N is given by

$$\theta = \theta_c + \arctan((N_c - N)\Delta x/D) \quad , \tag{4}$$

where θ_c is the Bragg angle corresponding to the central channel number N_c of the detector. Δx is the distance between two adjacent channels, and D is the distance between the crystal and the detector. The arctangent is used because the detector is oriented perpendicular to the line connecting the crystal and the center of the detector (see Fig. 3). The center position

of a line is obtained from a least squares fit of Gaussian functions to the experimental data. If the center position of a given line is known, its wavelength can be determined with respect to a reference line from Eqs. (2) and (4).

In the present measurement we have made all wavelength determinations with respect to the wavelength of the heliumlike resonance line w, since this value has been measured in several experiments (Briand *et al.* 1982; Beiersdorfer *et al.* 1989b) with high precision, i.e., better than 30 ppm. In the following, we have adopted a value of $\lambda = 1.85030$ Å for the wavelength of w, which represents an average of the value of 1.85028 Å obtained by Briand *et al.* (1982) and the value of 1.85031 Å obtained by Beiersdorfer *et al.* (1989b).

The error in our wavelength measurements depends largely on uncertainties in the value of the spectral dispersion $\Delta x/D$. This value is known to within 2.0×10^{-3}. Thus the uncertainty of the measured wavelengths is largest for lines which are situated farthest from w. Due to the good counting statistics, the statistical error for the center position contributes very little to the overall uncertainty in the measured wavelength of all but the weakest lines. The total estimated experimental error associated with the determination of the wavelength of each line or group of lines is given in Tables I–VI. Our error estimates are in general larger than those quoted in the tables of SFS, despite our somewhat better spectral resolution. This may be in part due to the fact that our estimates include uncertainties from our instrumental dispersion. The uncertainties quoted by SFS represent standard deviations for eight different measurements, and systematic errors due to instrumental effects, though discussed in their paper, are not included in their error limits.

The accuracy with which a given line can be determined will be reduced if it blends with one or more transitions in the same or in neighboring charge states. To identify spectral features that comprise more than one line, we have relied extensively on our model calculations. Many spectral features are indeed found to be blends and are identified as such in the Tables. Another limitation on the accuracy with which the wavelength of a given transition can be determined results from the possible presence of unresolved satellite lines. Unresolved satellites are produced by the dielectronic capture of an electron into an atomic level with quantum number $n \geq 3$ (Bely-Dubau *et al.* 1979; Bitter *et al.* 1981; Lemen *et al.* 1984; Beiersdorfer *et al.* 1992a,b,c). These unresolved satellites occur mainly on the long-wavelength side of a resonance line and have the effect of increasing the observed wavelength of the apparent line. The intensity of these satellites is temperature dependent and is largest for low electron temperatures. Among the transitions in Fe XXV, lines w and y are the most strongly affected by the presence of unresolved satellites (Beiersdorfer *et al.* 1992a,b,c). Among the transitions in Fe XXIV lines q and r are most strongly affected

(Lemen *et al.* 1984; Beiersdorfer *et al.* 1991a). A quantitative theoretical study of this effect has been given by Bitter *et al.* (1985), where the wavelength shift of the apparent $K\alpha$ line of helium-like titanium was studied as a function of electron and ion temperatures. They found a wavelength shift of ≤ 0.1 mÅ at electron and ion temperatures of 1 keV. Although we are unaware of any theoretical or experimental study that describes the effects of high-n, unresolved satellite lines on any of the transitions in Fe XXIII–XVIII, we presume that their presence might cause similar uncertainties in the wavelengths of the n=2 Kα lines in these lower-charged ion species.

In the following we give a detailed discussion of our measurements and compare the results with those from the solar flare observations of SFS. We have determined the line positions of all features marked in Fig. 7.

B. Transitions in the Region 1.850 – 1.870 Å: Lines w through z

The region between 1.850 Å and 1.870 Å contains all transitions in Fe XXV and most transitions of Fe XXIV. The heliumlike transitions w, x, y, and z are easily identified, and our experimental wavelengths agree well with those of SFS, as seen from Table I. They also agree within error limits with a recent measurement on the TFTR tokamak by Bitter *et al.* (1988). Setting the reference wavelength of w to 1.8503 Å, they report the wavelength of x, y, and z to be equal to 1.8553 Å, 1.8593 Å, and 1.8680 Å, respectively.

Among the lithiumlike transitions only q and j do not blend with other intense transitions, and their wavelengths can be determined with the highest certainty. Transition t blends with m, and k blends with r, while a overlaps with both k and q. Although dielectronic recombination excites k with a rate almost ten times the rate of r, r is almost as intense as k both in the intermediate-density and low-density limit. This is because r derives much of its intensity from innershell excitation, having an electron-impact excitation cross section exceeded only by that of q among the lithiumlike transitions, while k is excited purely by dielectronic recombination.

It is interesting to note the lithiumlike line l and especially the two berylliumlike lines $E1$ and $E2$, which are predicted to be located between j and z. While these lines have not yet been identified, they may play a role in cold plasmas where the ionization balance favors Fe XXIII. Ascertaining their exact positions would be very important, as it is conceivable that l and $E2$ blend with z and considerably enhance its apparent intensity in low-temperature plasmas. Such measurements may be possible, for example, in ion trap or storage ring facilities where one ionization stage or one excitation process can be studied at a time, as

demonstrated recently in measurements of the Kα satellite spectrum of heliumlike vanadium V XXII from an electron beam ion trap (Beiersdorfer *et al.* 1991a).

C. Transitions in the Region 1.870 – 1.881 Å: Lines $E3$ through $B2$

The wavelength region 1.870 – 1.881 Å contains most of the berylliumlike transitions. The most intense of these transitions is labeled $E3$ in Table II. It is predominantly excited by innershell excitation and is commonly refered to as line β.

The broad feature near 1.873 Å appears to be comprised of two lines, one centered around 1.8725 Å and the other around 1.8735 Å. SFS identify them as the $^3P_1 - ^3D_1$ and $^3P_1 - ^3D_2$ transitions, labeled $E6$ and $E8$ in Table II. Our model calculations show that this feature splits into two *groups* of lines, the first comprised of $E6$, e, and $E7$, the second comprised of $E8$, u, and $E9$. While $E8$ dominates the group at 1.8735 Å, contributing about two thirds of the total intensity, $E6$ does not dominate the other. For hot plasma conditions with a high abundance of Fe XXIV, the lithiumlike line e contributes more to the feature's intensity than does $E6$. Furthermore, Lemen *et al.* (1984) showed that the overall feature is enhanced by satellite transitions with high-n spectator electrons.

Our model calculations agree with SFS's identification of the feature at 1.8757 Å, labeled $E12$ in Table II, and of the feature at 1.8781 Å, labeled $E15$. SFS identify the adjacent feature on the long-wavelength side of $E15$ as the $^1S_0 - ^3P_1$ transition labeled $E16$. Our measurements show that this feature is broader than expected if it were comprised of only one line, and our model calculations predict that this feature is mainly due to the boronlike transition $B2$ instead. As the calculated intensities in Table II indicate, $B2$ dominates this feature even in hot and low-density plasmas.

D. Transitions in the Region 1.881 – 1.890 Å: Lines $B3$ through $E17$

This region is entirely dominated by boronlike transitions. SFS have identified two boronlike transitions in their spectra, i.e., the lines labeled $B5$ and $B6$ in Table III. By contrast, we identify contributions from six boronlike lines in this wavelength region.

In the last section we have shown that the feature that SFS identify as the berylliumlike transition $E16$ consists predominantly of the boronlike transition $B2$. Similarly, the feature at 1.8868 Å identified by SFS as the berylliumlike line $E17$ consists predominantly of the boronlike transition $B8$. In our spectra this feature is produced by a blend of $B7$ and $B8$. $E17$ might be situated on the long-wavelength side of $B7$ and $B8$, but it is too weak to be seen. Even in the low-density limit this feature is predicted to have a large contribution

from $B8$. We also note that identifying this feature as a blend of boronlike lines instead of the berylliumlike line $E17$ in the flare spectra significantly increases agreement between measured and calculated wavelengths in the data presented by SFS.

We also find that the feature at 1.882 Å consists of three lines: $B3$ at 1.8817 Å on one side, and the blend of $B4$ and $B5$ at 1.8826 Å on the other. SFS ascribe this feature solely to $B5$. As in our data, the feature in their flare spectrum appears wider than a single line width and seems blended with $B3$ and $B4$ as well. This conclusion is also supported by our intensity calculations in the low-density limit.

The only isolated boronlike line in the spectrum is $B6$ at 1.8853 Å. This is true also for the flare spectra. The width of this line can thus be used for comparison with neighboring lines to check whether or not they are broadened by blends.

E. Transitions in the Region 1.890 – 1.900 Å: Lines $C1$ through $C16$

The wavelength region between 1.890 Å and 1.900 Å exhibits four strong peaks. The most distinct is the peak at 1.8968 Å, which we attribute to the blend of the carbonlike lines $C11$, $C12$, and $C13$. The predicted position of the lithiumlike line o also coincides with the observed peak. Its intensity, however, is predicted to be much too weak to be significant. The other three peaks overlap and are situated between 1.8922 Å and 1.8945 Å. The first at 1.8922 Å consists of a blend of the boronlike line $B9$, the lithiumlike line p, and several carbonlike lines, of which $C5$ is the strongest. The second at 1.8933 Å consists of the two carbonlike lines $C6$ and $C7$; the third at 1.8945 Å consists of $C8$ and $C9$. In addition to these four peaks, we find a small shoulder on both their short-wavelength and long-wavelength sides, which we attribute to the carbonlike lines $C1$ and $C14$, respectively.

The solar flare data in this region reported by SFS look similar to ours, and thus they do not appear to be well described by our model calculations in the low-density limit. The low-density calculations, for example, predict $C9$ to dominate the region, while $C6$ and $C7$ are predicted to be virtually absent. An inspection of the data clearly does not support these predictions. On the other hand, the intermediate-density approximation does not fully describe the solar data either. Instead, an appropriate description seems to fall somewhere between the intermediate-density and low-density limits. Consequently, we believe that the peak at 1.8933 Å in the solar spectra consists of a blend of $C6$ and $C7$, as it does in the tokamak spectra. Similarly, the peak at 1.8968 Å most likely consists of a blend of $C12$ and $C13$ (and perhaps of $C14$). This supposition is supported by earlier predictions by Phillips *et al.* (1983), who computed large contributions not only from $C9$ and $C12$ but also from

$C6$ and $C13$ for plasmas with an electron density of 10^{11} cm^{-3}.

From our predictions, both in the low-density and in the intermediate-density limit, it is doubtful that the lithiumlike lines o and p can be resolved in solar flare data. In principle, it is conceivable that p may be observed free of blends with $B9$ or $C3$, as either of the latter lines has only a moderate intensity; however, p itself is a weak line, and to observe p would be possible only in very hot plasmas, where not only the carbonlike but also the boronlike ionization stages have negligible abundances. It is still more difficult to observe o because it blends with the very strong carbonlike lines $C12$ and $C13$. To our knowledge, the only unambiguous observation of lines o and p in iron was reported from measurements on an electron beam ion trap (Beiersdorfer *et al.* 1991b). In these measurements the energy of the electron beam was set to a value that corresponded to the resonance energy for dielectronic capture by the heliumlike iron ion into its $1s2s^2$ upper level. At this electron energy only these two lines were excited. Thus, o and p were observed free of blends, resulting in a test of the effect of relativity on their radiative branching ratio (Beiersdorfer *et al.* 1991b).

F. Transitions in the Region 1.900 – 1.910 Å: Lines $C17$ through $N13$

The cluster of lines in the wavelength region between 1.900 Å and 1.910 Å is mostly due to transitions in nitrogenlike iron. The peak at 1.9081 Å is dominated by the nitrogenlike transition $N11$; it also receives a small contribution from $N12$. The other strong peak in the spectrum at 1.9056 Å seems to be formed by the nitrogenlike transitions $N6$ and $N7$. The remainder of the overall feature in this spectral range is comprised of unresolved contributions from the nitrogenlike transitions $N1$, $N2$, $N3$, $N5$, $N8$, $N9$, and $N10$. A small, almost fully resolved feature is found on the short-wavelength side at 1.9017 Å, which we ascribe to the carbonlike transition $C17$.

The appearance of the predicted emission spectrum in this wavelength range depends sensitively on the values of the wavelength employed for each transition in the model calculations. The values, which we use to generate the model spectra and which we give in Table V, have been adjusted from the values given by SFS to match the observed shape of this spectral region. Although we have achieved a good match with only minor adjustments in the wavelength values, we note that our set of wavelength values is not unique and that different combinations of wavelength values can be found that would generate theoretical emission spectra in good agreement with observations, especially since the exact shape of the nitrogenlike emission spectrum also depends sensitively on the electron density, as discussed below. Consequently, the identification of the weak nitrogenlike transitions in this wave-

length range will remain tenuous until either high precision energy level calculations or very high resolution spectral observations become available to distinguish individual nitrogenlike lines.

Like the Fe XXI emission, the Fe XX emission is very sensitive to the electron density. In the low-density approximation, $N11$ is by far the strongest feature followed by $N5$ (cf. Table V). As the density increases, the intensity of $N11$ drops off, and $N6$ becomes the strongest line. In the high-density regime, $N2$ and $N3$ become major contributors to the emission, and the relative importance of $N11$ diminishes further. This behavior is supported by the calculations of Phillips *et al.* (1983) and of Lemen *et al.* (1986), who computed the line intensities at densities of 10^{11} cm^{-3}, 10^{13} cm^{-3}, and 10^{15} cm^{-3}. The strong sensitivity to the electron density explains why our measured value of the relative intensity of $N11$ and of the blend $N6$ and $N7$ is larger than our predictions: The measured electron density never exceeds 2×10^{13} cm^{-3}, while the intermediate-density approximation assumes a relative distribution of ground-state fine-structure level populations that may be appropriate at somewhat higher densities near 10^{14} cm^{-3}. Model calculations incorporating an explicit density-dependent determination of these level populations for several intermediate densities would be needed to accurately describe the observed emission.

The solar spectra reveal features similar to ours. SFS identified two features in their spectra, i.e., the lines we label $N5$ and $N11$. In the low-density approximation, these two lines produce by far the strongest predicted features. Other nitrogenlike transitions are predicted to contribute to the emission in this range as well, such as $N4$ and $N7$. Indeed, the flare data of SFS show two distinct peaks, which are situated on the short-wavelength side of the peak ascribed to $N5$ by SFS and which were not identified. The lower energy peak of the two may well correspond to $N2$, while the higher may correspond to $C17$.

G. Transitions in the Region 1.910 – 1.940 Å: Lines $N14$ through $F2$

The wavelength region above 1.910 Å contains the weakest features in the emission spectra we observed. The region harbors all oxygenlike transitions in addition to two fluorinelike and a few nitrogenlike transitions. Like the model predictions in the wavelength region between 1.900 Å and 1.910 Å, the model predictions in this wavelength region are uncertain. Again, the Fe XIX emission depends sensitively on electron density, and small changes in the theoretical wavelength data result in very differently shaped spectra. Nevertheless, using the wavelength data listed in Table VI, we have been able to match the observed intensities reasonably well. The only exception is the intensity of the oxygenlike lines $O1$ and $O3$

compared to that of $O4$, which is overestimated in the theoretical spectra in Figs. 4(b) and 5(b). We note that $O3$ rapidly loses intensity as the density is decreased. Like the ratio of $N11$ and the blend of $N6$ and $N7$ discussed in the previous section, the difference may be the result of overestimating the electron density in the model calculations.

Comparing the theoretical spectra with observations, we identify seven features in the data. The shortest-wavelength peak at 1.9136 Å we ascribe to the nitrogenlike transition $N14$. The feature next to it we ascribe to the blend of oxygenlike lines $O1$, $O2$, and $O3$, followed by a peak produced by $O4$. Our model also predicts observable intensities for $O7$ and $O9$, and we have identified two features in our spectra that may correspond to these two transitions.

Only two Kα transitions are allowed in fluorinelike ions. These are predicted to have very small intensities because only a small fraction of all iron ions are in the fluorinelike ionization stage at the electron temperature prevalent in our tokamak plasmas. Nevertheless, we have been able to identify two features in our data that we can ascribe to the fluorinelike transitions. These are located at 1.9264 Å and 1.9305 Å. The wavelengths of these features agree reasonably well with those predicted by the RAC code if one takes into account the fact that the RAC code generally underestimates the wavelengths of transitions in this wavelength region.

The solar spectra contain several features in this wavelength region. SFS tentatively identified one oxygenlike transition and one fluorinelike transition in their spectra. In the low-density approximation, transition $O4$ forms the strongest oxygenlike line, and it is this transition that SFS assign to a feature at 1.9175 Å. This agrees well with the value of 1.9170 Å that we find in our measurements. The identification of the fluorinelike transition $F1$ in the solar data, however, appears incorrect. SFS find a value of 1.9215 Å, which is 5 mÅ shorter than our value of 1.9264 Å and which is much closer to $O7$ than to $F1$.

From the results of our model calculations we expect to find the nitrogenlike transition $N15$ in the solar data. In the low-density approximation, it is predicted to be the strongest of nitrogenlike transitions that fall into this wavelength region. The solar spectrum of SFS indeed show a feature, situated on the short-wavelength side of $O4$ at about 1.914 Å, which is a suitable candidate.

VI. Summary and Discussion

We have presented a detailed analysis of the Kα spectrum of iron from tokamak plasmas that contains all ionization stages from Fe XVIII through Fe XXV. We have identified 40

features consisting either of single or multiple lines, several of which were identified for the first time, and determined their wavelengths with high accuracy. This compares with 27 features described in the solar flare spectra of Seely, Feldman, and Safronova (1986). The increase is the result of better counting statistics and better resolution, as well as the presence of transitions that are not excited in the lower-density solar plasmas.

Our analysis was aided by accurate knowledge of the plasma conditions, as electron temperature and density were measured independently with non-spectroscopic techniques. In addition, we performed model calculations to predict synthetic emission spectra for comparison with our observations. The model incorporates electron collision and dielectronic recombination rates that result in the excitation of the $1s2s^r2p^s$ configuration and uses the ion abundances derived from a balance of ionization and recombination for radially varying temperature and density profiles. Very good overall agreement between the model calculations and the oberservations was obtained, which gives us confidence in our line identifications and spectral modeling capabilities. As a result, we were able to point out several spectral features that are formed by transitions different from those reported in earlier analyses.

The model calculations exhibit a strong sensitivity of the Fe XXII, Fe XXI, Fe XX, and Fe XIX line emission on electron density. This sensitivity arises from differences in the fine-structure level populations of the ground states of the initial ion undergoing electron-impact excitation or dielectronic recombination. Our present model uses a simplified treatment of the initial ground state population, which is assumed to be statistically distributed among all ground state fine-structure levels. This approximation is shown to yield adequate predictions of the overall line emission. A detailed modeling of the density dependence of the initial (and excited) state distributions, however, is needed to describe with high precision all individual line intensities. In particular, we have found that the tokamak density is less than necessary for the assumption of a statistical distribution among ground-state fine-structure levels to be fully valid. Similarly, the full validity of the low-density assumption that only the lowest fine-structure level is populated requires an electron density lower than that found in solar flares. Because of the strong sensitivity of the Kα line emission to electron density, future models that include a detailed treatment of all density effects will be able to provide the capability necessary to accurately infer the electron density from observations.

The model calculations also exhibit a strong sensitivity to the assumed line positions. This is because many lines blend, especially those of the lower charge states of iron. Small changes (< 0.5 mÅ) in the assumed line position thus leads to a large difference in the shape of a given emission feature. This means that our line identifications of some of the

weaker transitions are tentative. More precise calculations of the transition energies are needed for unambiguous identification. Presently, the needed accuracy, which is on the order of the quantum electrodynamical and residual electron-electron correlation energies, exceeds that obtainable in available calculations. Alternatively, the transition energies could be measured with very high-resolution spectroscopy on advanced laboratory x-ray sources, such as electron beam ion traps, where line overlap and blending can be reduced or eliminated by our choosing the ionization stage and excitation process of interest.

The identity of the Fe XXV transitions w, x, y, and z is well established, and we did not include them into our model. These lines play, however, an important role in plasma diagnostics and are used, for example, for inferring the electron temperature. For this application, it is necessary to model the intensities of these lines with high accuracy. Our model indicates that z, for example, may overlap the berylliumlike line $E2$ and the lithiumlike satellite l. As these two lines could be intense in cool plasmas, these lines must be included in models used to analyze the heliumlike lines. Again, future investigations must ascertain the positions of these lines.

In conclusion we note that our ionization balance calculations took into account the effects of diffusive ion transport. All calculations we presented assumed a diffusion coefficient of 3000 cm^2/sec. This value provided the best agreement between synthetic and observed spectra. Not as good, but reasonable agreement was also achieved for values between 2000 cm^2/sec and 5000 cm^2/sec. Because the model calculations are sensitive to ion transport, we can use them for plasma diagnostics. By computing a series of synthetic spectra for different diffusion coefficients until the best agreement with observation is attained, we can infer the magnitude of the ion transport. The value of 3000 cm^2/sec thus represents a measurement of the diffusion coefficient, and 2000 cm^2/sec and 5000 cm^2/sec represent the accuracy limits.

Acknowledgments

This work was performed under the auspices of the U. S. Department of Energy by the Lawrence Livermore National Laboratory under contract No. W-7405-ENG-48 and by the Princeton Plasma Physics Laboratory under contract No. DE-AC02-76-CHO-3073. Two of the authors (PB and SMK) were supported by the National Aeronautics and Space Administration under grant NAGW-2688 from the X-Ray Astronomy Research and Analysis Program; a third (VLJ) received support from the U. S. Department of Energy, Office of Fusion Energy.

REFERENCES

Beiersdorfer, P., von Goeler, S., Bitter, M., Hill, K. W., Hulse, R. A., and Walling, R. S., 1989a, *Rev. Sci. Instrum.*, **60**, 895.

Beiersdorfer, P., Bitter, M., von Goeler, S., and Hill, K. W., 1989b, *Phys. Rev. A.*, **40**, 150.

Beiersdorfer, P., Bitter, M., von Goeler, S., and Hill, K. W., 1989c, *Nucl. Instrum. Methods B*, **43**, 347.

Beiersdorfer, P., Marrs, R., Henderson, J., Knapp, D., Levine, M., Platt, D., Schneider, D., Vogel, D., and Wong, K., 1990, *Rev. Sci. Instrum.*, **61**, 2338.

Beiersdorfer, P., Chen, M. H., Marrs, R. E., Schneider, M. B., and Walling, R. S., 1991a, *Phys. Rev.* A, **44**, 396.

Beiersdorfer, P., Chen, M. H., MacLaren, S., Marrs, R. E., Vogel, D. A., Wong, K., and Zasadzinski, R., 1991b, *Phys. Rev. A*, **44**, 4730.

Beiersdorfer, P., Cauble, R., Chantrenne, S., Chen, M., Knapp, D., Marrs, R., Phillips, T., Reed, K., Schneider, M., Scofield, J., Wong, K., Vogel, D., Zasadzinski, R., Wargelin, B., Bitter, M., and von Goeler, S., 1992a, in *Electron and Atomic Collisions, Invited Papers, XVII ICPEAC, Brisbane, Australia, July 10-16, 1991*, edited by MacGillivray, W. R., McCarthy, I. E., and Standage, M. C., (New York: Adam Hilgar), p. 313.

Beiersdorfer, P., Chantrenne, S., Chen, M. H., Marrs, R. E., Vogel, D. A., Wong, K. L., and Zasadzinski, R., 1992b, *Zeitschrift f. Physik D*, **21**, S209.

Beiersdorfer, P., Schneider, M. B., Bitter, M., and von Goeler, S., 1992c, *Rev. Sci. Instrum.*, in press.

Beiersdorfer, P., Phillips, T. W., Wong, K. L., Marrs, R. E., and Vogel, D. A., 1992d, submitted to *Phys. Rev. A.*

Bely-Dubau, F., Gabriel, A. H., and Volonté, S., 1979, *Mon. Not. R. Astron. Soc.*, **189**, 801.

Bitter, M., von Goeler, S., Horton, R., Goldman, M., Hill, K., Sauthoff, N. R., and Stodiek, W., 1979a, *Phys. Rev. Lett.*, **42**, 304.

Bitter, M., Hill, K. W., Sauthoff, N. R., Efthimion, P. C., Merservey, E., Roney, W., von Goeler, S., Horton, R., Goldman, M., and Stodiek, W., 1979b, *Phys. Rev. Lett.*, **43**, 129.

Bitter, M., von Goeler, S., Hill, K., Horton, R., Johnson, D., Roney, W., Sauthoff, N., Silver, E., and Stodiek, W., 1981, *Phys. Rev. Lett.*, **47**, 921.

Bitter, M., Hill, K. W., Zarnstorff, M., von Goeler, S., Hulse, R., Johnson, L. C., Sauthoff, N. R., Sesnic, S., and Young, K. M., 1985, *Phys. Rev. A*, **32**, 3011.

Bitter, M., Hsuan, H., Rice, J. E., Hill, K. W., Diesso, M., Grek, B., Hulse, R., Johnson, D. W., Johnson, L. C., and von Goeler, S., 1988, *Rev. Sci. Instrum.*, **59**, 2131.

Bitter, M., Hsuan, H., Decaux, V., Grek, B., Hill, K. W., Hulse, R., Kruegel, L. A., Johnson, D., von Goeler, S., and Zarnstorff, M., 1991, *Phys. Rev. A*, **44**, 1796.

Briand, J. P., 1982, in *X-rays and Atomic Inner-Shell Physics - 1982*, AIP Conference Proceedings No. 94, edited by B. Crasemann (New York: AIP), p. 271.

Briand, J. P., Tavernier, M., Indelicato, P., Marrus, R., and Gould, H., 1983, *Phys. Rev. Lett.*, **50**, 832.

Brown, C. M., Feldman, U., Doschek, G. A., Seely, J. F., LaVilla, R. E., Jacobs, V. L., Henderson, J. R., Knapp, D. A., Marrs, R. E., Beiersdorfer, P., and Levine, M. A., 1989, *Phys. Rev. A*, **40**, 4089.

Cowan, R. D., *The Theory of Atomic Structure and Spectra*, (Berkeley: University of California Press).

Compton, A. H. and Allison, S. K., 1935, X-Rays in Theory and Experiment, 2nd Edition (Princeton: van Nostrand).

Doschek, G. A., Feldman, U., Cowan, R. D., 1981, *Astrophys. J.*, **245**, 315.

Doschek, G. A., 1990, in *X-ray and Inner-Shell Processes, Knoxville, TN 1990*, AIP Conference Proceedings No. 215, edited by Carlson, T. A., Krause, M. O., and Manson, S. T. (New York: AIP), p. 603.

Fabian, A. C. and George I. M., 1991, in *Iron Line Diagnostics in X-Ray Sources*, Lecture Notes in Physics, edited Treves, A., Perola, G. C., and Stella, L, (Berlin: Springer-Verlag), p. 169.

Feldman, U. , Doschek, G. A., and Kreplin, R. W., 1980, *Astrophys. J.*, **238**, 365.

Gabriel, A. H., 1972, *Mon. Not. R. Astron. Soc.*, **160**, 99.

Grant, I. P., McKenzie, B. J., Norrington, P. H., Mayers, D. F., and Pyper, N. C., 1980, *Comput. Phys. Commun.*, **21**, 207.

Grineva, Yu. I., Karev, V. I., Korneev, V. V., Krutov, V. V., Mandelstam, S. L., Vainshtein, L. A., Vasilyev, B. N., and Zhitnik, I. A., 1973, *Sol. Phys.*, **29**, 441.

Hill, K. W., von Goeler, S., Bitter, M., Campbell, L., Cowan, R. D., Fraenkel, B., Greenberger, A., Horton, R., Hovey, J., Roney, W., Sauthoff, N. R., and Stodiek, W., 1979, *Phys. Rev. A*, **19**, 1770.

Hulse, R. A., 1983, *Nucl. Technol./Fusion*, **3**, 259.

Jacobs, V. L., Doschek, G. A., Seely, J. F., and Cowan, R. D., 1989, *Phys. Rev. A*, **39**, 2411.

Korneev, V. V., Krutov, V. V., Mandelstram, S. L., Urnov, A. M., Zhitnik, I. A., Kononov, A. Ya., Sylwester, B., and Sylwester, J., 1979, *Solar Phys.*, **63**, 319.

Lemen, J. R., Phillips, K. J. H., Cowan, R. D., and Grant, I. P., 1984 *Astron. Astrophys.*, **135**, 313.

Lemen, J. R., Phillips, K. J. H., Doschek, G. A., and Cowan, R. D., 1986, *J. Appl. Phys.*, **60**, 1960.

Lie, T. N. and Elton, R. C., 1971, *Phys. Rev. A*, **3**, 865.

Mason, H. E., Doschek, G. A., Feldman, U., and Bhatia, A. K., 1979, *Astron. Astrophys.*, **73**, 74.

Mitchell, R. J., Culhane, J. L., Davison, P. J. N., and Ives, J. C., 1976, *Mon. Not. Roy. Astr. Soc.*, **175**, 29.

Orlinskij, D. V. and Magyar, G., 1988, *Nucl. Fusion*, **28**, 611.

Phillips, K. J. H., Lemen, J. R., Cowan, R. D., Doschek, G. A., and Leibacher, J. W., *Astrophys. J.*, **265**, 1120.

Post, D. E., Jensen, R. V., Tartar, C. B., Grasberger, W. H., and Lokke, W. A., 1977, *At. Data Nucl. Data Tables*, **20**, 397.

Scofield, J. H., 1991, *Phys. Rev. A*, **44**, 139.

Seely, J. F., Feldman, U., and Safronova, U. I., 1986, *Astrophys. J.*, **304**, 838.

Serlemitsos, P. J., Smith, B. W., Boldt, E. A., and Swank, J. H., 1977, *Astrophys. J.*, **211**, L63.

Tsunemi, H., Yamashita, K., Masai, K., Hayakawa, S., and Koyama, K., 1986, *Astrophys. J.*, **306**, 248.

Tsuru, T., Makishima, K., Ohashi, T., Inoue, H., Koyama, K., Turner, M. J. L., Barstow, M. A., McHardy, I. M., Pye, J. P., Tsunemi, H., Kitamoto, S., Taylor, A. R., and Nelson, R. F., 1989, *Publ. Astron. Soc. Japan*, **41**, 679.

Ulmer, M. P., Cruddace, R. G., Fenimore, E. E., Fritz, G. G., and Snyder, W. A., 1987, *Astrophys. J.*, **319**, 118.

von Goeler, S., 1979, in *Proceedings of the Course on Diagnostics for Fusion Experiments, Varenna, Italy, 1978*, edited by Sindoni, E. and Wharton, C. (New York: Pergamon Press) p. 79.

White, N. E., Culhane, J. L., Parmar, A. N., Kellett, B. J., Kahn, S., van den Oord, G. H. J., and Kuijpers, J., 1986, *Astrophys. J.*, **301**, 262.

White, N. E., Peacock, A., and Taylor, B. G., 1985, *Astrophys. J.*, **296**, 475

Wyckoff, R. W. G., 1963, *Crystal Structures*, 2nd ed. Vol I (New York: Wiley).

TABLE I. Line identification of features in the wavelength region 1.850 – 1.870 Å, which contains predominantly transitions from Fe XXV and Fe XXIV. I_{cold} and I_{hot} denote relative theoretical intensities for the plasma conditions shown in Fig. 1 calculated in the intermediate-density approximation. I_{low} denotes relative theoretical intensities for the "cold" plasma condition shown in Fig. 1 calculated in the low-density approximation. All wavelength values are in Ångstroms. Uncertainties in the measured wavelengths are in parentheses. ⟨⟩ denotes blends.

Label	Ion	Transition	I_{cold}	I_{hot}	I_{low}	λ^a_{expt}	λ^b_{expt}	λ^c_{theo}	λ^d_{theo}
w	Fe XXV	$1s^2\ ^1S_0 - 1s2p\ ^1P_1$				1.85030	1.85030	1.85046	
x	Fe XXV	$1s^2\ ^1S_0 - 1s2p\ ^3P_2$				1.85537(9)	1.85528(8)		
s	Fe XXIV	$1s^22s\ ^2S_{1/2} - 1s2s2p\ ^2P_{3/2}$	1.7	3.2	1.5			1.85625	
m	Fe XXIV	$1s^22p\ ^2P_{3/2} - 1s2p^2\ ^2S_{1/2}$	7.6	15.1	6.9	⟨1.85693(20)⟩		1.85685	
t	Fe XXIV	$1s^22s\ ^2S_{1/2} - 1s2s2p\ ^2P_{1/2}$	16.6	33.3	15.0	⟨1.85693(20)⟩	1.85688(7)	1.85715	
y	Fe XXV	$1s^2\ ^1S_0 - 1s2p\ ^3P_1$				1.85942(10)	1.85945(22)		
q	Fe XXIV	$1s^22s\ ^2S_{1/2} - 1s2s2p\ ^2P_{3/2}$	48.5	100.0	44.0	1.86104(15)	1.86092(14)	1.86105	
a	Fe XXIV	$1s^22p\ ^2P_{3/2} - 1s2p^2\ ^2P_{3/2}$	10.0	19.8	9.1	1.86207(30)	1.86208(39)	1.86225	
k	Fe XXIV	$1s^22p\ ^2P_{1/2} - 1s2p^2\ ^2D_{3/2}$	27.1	53.6	24.6	⟨1.86325(20)⟩	1.86312(16)	1.86315	
r	Fe XXIV	$1s^22s\ ^2S_{1/2} - 1s2s2p\ ^2P_{1/2}$	18.9	38.3	17.1	⟨1.86325(20)⟩		1.86355	
j	Fe XXIV	$1s^22p\ ^2P_{3/2} - 1s2p^2\ ^2D_{5/2}$	41.2	81.9	37.4	1.86576(12)	1.86582(4)	1.86595	
$E1$	Fe XXIII	$1s^22s2p\ ^3P_2 - 1s2s2p^2\ ^3S_1$	4.4	3.4	4.0			1.86685	1.8663
l	FeXXIV	$1s^22p\ ^2P_{3/2} - 1s2p^2\ ^2D_{3/2}$	2.9	5.7	2.6			1.86755	
$E2$	Fe XXIII	$1s^22s2p\ ^3P_2 - 1s2s2p^2\ ^1D_2$	8.1	6.3	7.4			1.86795	1.8678
z	Fe XXV	$1s^2\ ^1S_0 - 1s2s\ ^3S_1$				1.86812(11)	1.868799(10)		

[a]present measurement; all wavelengths are determined relative to λ=1.85030 Å of line w.

[b]measurements of Seely, Feldman, and Safronova (1986); wavelengths are shifted by 0.16 mÅ in accordance with our choice of reference wavelength.

[c]semiempirical results from Z-expansion calculation of Seely, Feldman, and Safronova (1986); values used in generating our synthetic spectra.

[d]present calculation using the RAC code.

TABLE II. Line identification of features in the wavelength region 1.870 – 1.881 Å, which contains predominantly transitions from Fe XXIII. I_{cold} and I_{hot} denote relative theoretical intensities for the plasma conditions shown in Fig. 1 calculated in the intermediate-density approximation. I_{low} denotes relative theoretical intensities for the "cold" plasma condition shown in Fig. 1 calculated in the low-density approximation. All wavelength values are in Ångstroms. Uncertainties in the measured wavelengths are in parentheses. ⟨⟩ denotes blends.

Label	Ion	Transition	I_{cold}	I_{hot}	I_{low}	λ^a_{expt}	λ^b_{expt}	λ^c_{theo}	λ^d_{theo}
$E3(\beta)$	FeXXIII	$1s^22s^2\ ^1S_0 - 1s2s^22p\ ^1P_1$	99.7	92.0	90.4	1.87035(8)	1.87035(11)	1.87045	1.8701
$E4$	FeXXIII	$1s^22s2p\ ^1P_1 - 1s2s2p^2\ ^1S_0$	2.5	1.9	2.2			1.87075	1.8699
$E5$	FeXXIII	$1s^22s2p\ ^3P_2 - 1s2s2p^2\ ^3S_1$	2.1	1.6	1.9			1.87155	1.8705
$E6$	FeXXIII	$1s^22s2p\ ^3P_1 - 1s2s2p^2\ ^3D_1$	14.5	11.1	13.1	⟨1.87246(35)⟩	1.87226(23)	1.872[illegible]	1.8719
e	FeXXIV	$1s^22p\ ^2P_{3/2} - 1s2p^2\ ^4P_{5/2}$	6.6	13.0	5.9	⟨1.87246(35)⟩		1.87275	
$E7$	FeXXIII	$1s^22s2p\ ^3P_0 - 1s2s2p^2\ ^3P_1$	7.0	5.3	6.4	⟨1.87246(35)⟩		1.87285	1.8730
$E8$	FeXXIII	$1s^22s2p\ ^3P_1 - 1s2s2p^2\ ^3D_2$	31.4	24.3	28.5	⟨1.87347(35)⟩	1.87347(15)	1.87355	1.8733
u	FeXXIV	$1s^22s\ ^2S_{1/2} - 1s2s2p\ ^4P_{3/2}$	1.8	3.6	1.6	⟨1.87347(35)⟩		1.87375	
$E9$	FeXXIII	$1s^22s2p\ ^3P_2 - 1s2s2p^2\ ^3P_2$	14.6	11.2	13.3	⟨1.87347(35)⟩		1.87385	1.8734
$E10$	FeXXIII	$1s^22s2p\ ^1P_1 - 1s2s2p^2\ ^3P_2$	5.3	4.1	4.8			1.87515	1.8747
$E11$	FeXXIII	$1s^22s2p\ ^3P_2 - 1s2s2p^2\ ^3D_1$	4.1	3.2	3.7			1.87575	1.8751
$E12$	FeXXIII	$1s^22s2p\ ^3P_2 - 1s2s2p^2\ ^3D_3$	49.1	37.9	44.6	1.87574(20)	1.87552(12)	1.87585	1.8753
$E13$	FeXXIII	$1s^22s2p\ ^3P_2 - 1s2s2p^2\ ^3D_2$	2.4	1.8	2.2			1.87675	1.8765
$E14$	FeXXIII	$1s^22s2p\ ^3P_2 - 1s2s2p^2\ ^3P_1$	2.0	1.5	1.8			1.87715	1.8773
$B1$	FeXXII	$1s^22s^22p\ ^2P_{1/2} - 1s2s^22p^2\ ^2P_{3/2}$	1.2	0.4	0.4			1.87720[e]	1.8771
$E15$	FeXXIII	$1s^22s2p\ ^1P_1 - 1s2s2p^2\ ^1D_2$	13.3	10.2	12.1	1.87812(20)	1.87798(14)	1.87755	1.8781
$E16$	FeXXIII	$1s^22s^2\ ^1S_0 - 1s2s^22p\ ^3P_1$	5.7	4.5	5.2	1.87933(30)	1.87957(25)[f]	1.87905	1.8787
$B2$	FeXXII	$1s^22s^22p\ ^2P_{3/2} - 1s2s^22p^2\ ^2S_{1/2}$	23.4	8.3	14.8	1.88018(30)		1.87995	1.8795

[a]present measurement; all wavelengths are determined relative to λ=1.85030 Å of line w.

[b]measurements of Seely, Feldman, and Safronova (1986); wavelengths are shifted by 0.16 mÅ in accordance with present choice of reference wavelength.

[c]semiempirical results from Z-expansion calculation of Seely, Feldman, and Safronova (1986); values used in generating our synthetic spectra.

[d]present calculation using the RAC code.

[e]estimate based on calculations with the RAC code.

[f]misidentified.

TABLE III. Line identification of features in the wavelength region 1.881 – 1.890 Å, which contains predominantly transitions from Fe XXII. I_{cold} and I_{hot} denote relative theoretical intensities for the plasma conditions shown in Fig. 1 calculated in the intermediate-density approximation. I_{low} denotes relative theoretical intensities for the "cold" plasma condition shown in Fig. 1 calculated in the low-density approximation. All wavelength values are in Ångstroms. Uncertainties in the measured wavelengths are in parentheses. ⟨⟩ denotes blends.

Label	Ion	Transition	I_{cold}	I_{hot}	I_{low}	λ^a_{expt}	λ^b_{expt}	λ^c_{theo}	λ^d_{theo}
$B3$	FeXXII	$1s^22s^22p\ ^2P_{3/2} - 1s2s^22p^2\ ^2P_{3/2}$	72.1	26.2	24.8	1.88168(35)		1.88185	1.8812
$B4$	FeXXII	$1s^22s^22p\ ^2P_{1/2} - 1s2s^22p^2\ ^2P_{1/2}$	23.2	8.6	48.9	⟨1.88258(15)⟩		1.88250[g]	1.8822
$B5$	FeXXII	$1s^22s^22p\ ^2P_{1/2} - 1s2s^22p^2\ ^2D_{3/2}$	81.4	28.5	100.0	⟨1.88258(15)⟩	1.88243(10)[e]	1.88255	1.8819
$B6$	FeXXII	$1s^22s^22p\ ^2P_{3/2} - 1s2s^22p^2\ ^2D_{5/2}$	100.0	34.5	79.6	1.88532(15)	1.88518(11)	1.88535	1.8846
$B7$	FeXXII	$1s^22s^22p\ ^2P_{3/2} - 1s2s^22p^2\ ^2P_{1/2}$	5.5	2.0	0.4	⟨1.88683(20)⟩		1.88680[g]	1.8864
$B8$	FeXXII	$1s^22s^22p\ ^2P_{3/2} - 1s2s^22p^2\ ^2D_{3/2}$	9.2	3.2	6.6	⟨1.88683(20)⟩		1.88675	1.8861
$E17$	FeXXIII	$1s^22s2p\ ^3P_2 - 1s2s2p^2\ ^5P_3$	2.2	1.7	2.0		1.88690(35)[f]	1.88745	1.8871

[a]present measurement; all wavelengths are determined relative to λ=1.85030 Å of line w.

[b]Seely, Feldman, and Safronova (1986); wavelengths are shifted by 0.16 mÅ in accordance with present choice of reference wavelength.

[c]semiempirical results from Z-expansion calculation of Seely, Feldman, and Safronova (1986); values used in generating our synthetic spectra.

[d]present calculation using the RAC code.

[e]identified as $B5$, but blends with $B3$ and $B4$.

[f]identified as $E17$, but is due to $B8$.

[g]estimate based on calculations with the RAC code.

TABLE IV. Line identification of features in the wavelength region 1.890 – 1.900 Å, which contains predominantly transitions from Fe XXI. I_{cold} and I_{hot} denote relative theoretical intensities for the plasma conditions shown in Fig. 1 calculated in the intermediate-density approximation. I_{low} denotes relative theoretical intensities for the "cold" plasma condition shown in Fig. 1 calculated in the low-density approximation. All wavelength values are in Ångstroms. Uncertainties in the measured wavelengths are in parentheses. ⟨⟩ denotes blends.

Label	Ion	Transition	I_{cold}	I_{hot}	I_{low}	λ^a_{expt}	λ^b_{expt}	λ^c_{theo}	λ^d_{theo}
$C1$	Fe XXI	$1s^22s^22p^2\ ^1D_2 - 1s2s^22p^3\ ^1P_1$	18.1	3.3	0.0	1.89080(40)		1.89145	1.8907
$C2$	Fe XXI	$1s^22s^22p^2\ ^3P_0 - 1s2s^22p^3\ ^3S_1$	1.2	0.2	0.7			1.89180[g]	1.8903
$B9$	Fe XXII	$1s^22s^22p\ ^2P_{3/2} - 1s2s^22p^2\ ^4P_{5/2}$	4.8	1.7	3.9	⟨1.89219(25)⟩		1.89205	1.8913
p	Fe XXIV	$1s^22p\ ^2P_{1/2} - 1s2s^2\ ^2S_{1/2}$	1.2	2.5	1.1	⟨1.89219(25)⟩	1.89244(7)[e]	1.89235	
$C3$	Fe XXI	$1s^22s^22p^2\ ^3P_1 - 1s2s^22p^3\ ^1D_2$	3.2	0.6	2.2	⟨1.89219(25)⟩		1.89240[g]	1.8910
$C4$	Fe XXI	$1s^22s^22p^2\ ^3P_1 - 1s2s^22p^3\ ^3P_0$	1.2	0.2	0.0	⟨1.89219(25)⟩		1.89255	1.8913
$C5$	Fe XXI	$1s^22s^22p^2\ ^3P_2 - 1s2s^22p^3\ ^3P_1$	15.6	2.8	5.6	⟨1.89219(25)⟩		1.8929:	1.8921
$C6$	Fe XXI	$1s^22s^22p^2\ ^3P_2 - 1s2s^22p^3\ ^1D_2$	31.1	5.5	2.5	⟨1.89332(25)⟩	1.89343(40)	1.89355	1.8926
$C7$	Fe XXI	$1s^22s^22p^2\ ^3P_1 - 1s2s^22p^3\ ^3S_1$	16.8	3.1	2.0	⟨1.89332(25)⟩		1.89385	1.8929
$C8$	Fe XXI	$1s^22s^22p^2\ ^1D_2 - 1s2s^22p^3\ ^3P_2$	39.9	7.1	3.3	⟨1.89445(25)⟩		1.89455	1.8936
$C9$	Fe XXI	$1s^22s^22p^2\ ^3P_0 - 1s2s^22p^3\ ^3D_1$	15.9	2.8	77.3	⟨1.89445(25)⟩	1.89458(18)	1.89475	1.8938
$C10$	Fe XXI	$1s^22s^22p^2\ ^3P_2 - 1s2s^22p^3\ ^3S_1$	7.0	1.3	0.8			1.89535	1.8945
$C11$	Fe XXI	$1s^22s^22p^2\ ^1S_0 - 1s2s^22p^3\ ^1P_1$	12.4	2.2	0.0	⟨1.89680(20)⟩		1.89625	1.8951
o	Fe XXIV	$1s^22p\ ^2P_{3/2} - 1s2s^2\ ^2S_{1/2}$	1.2	2.5	1.1	⟨1.89680(20)⟩	⟨1.89676(9)⟩[f]	1.89685	
$C12$	Fe XXI	$1s^22s^22p^2\ ^3P_1 - 1s2s^22p^3\ ^3D_2$	23.0	4.1	33.0	⟨1.89680(20)⟩	⟨1.89676(9)⟩[f]	1.89695	1.8958
$C13$	Fe XXI	$1s^22s^22p^2\ ^3P_2 - 1s2s^22p^3\ ^3D_3$	26.6	4.6	12.6	⟨1.89680(20)⟩		1.89735	1.8962
$C14$	Fe XXI	$1s^22s^22p^2\ ^1D_2 - 1s2s^22p^3\ ^1D_2$	10.5	1.9	0.9	1.89891(40)		1.89815	1.8972
$C15$	Fe XXI	$1s^22s^22p^2\ ^3P_2 - 1s2s^22p^3\ ^3D_1$	3.1	0.5	4.5			1.89885	1.8980
$C16$	Fe XXI	$1s^22s^22p^2\ ^1D_2 - 1s2s^22p^3\ ^3S_1$	1.2	0.2	0.1			1.90060[g]	1.9002

[a]present measurement; all wavelengths are determined relative to λ=1.85030 Å of line w.

[b]Seely, Feldman, and Safronova (1986); wavelengths are shifted by 0.16 mÅ in accordance with present choice of reference wavelength.

[c]semiempirical results from Z-expansion calculation of Seely, Feldman, and Safronova (1986); values used in generating our synthetic spectra.

[d]present calculation using the RAC code.

[e]identified as p, but blends with $B9$ and $C3$.

[f]identified as blend of o and $C12$, but also blends with $C13$.

[g]estimate based on calculations with the RAC code.

TABLE V. Line identification of features in the wavelength region 1.900 – 1.910 Å, which contains predominantly transitions from Fe XX. I_{cold} and I_{hot} denote relative theoretical intensities for the plasma conditions shown in Fig. 1 calculated in the intermediate-density approximation. I_{low} denotes relative theoretical intensities for the "cold" plasma condition shown in Fig. 1 calculated in the low-density approximation. All wavelength values are in Ångstroms. Uncertainties in the measured wavelengths are in parentheses. ⟨⟩ denotes blends.

Label	Ion	Transition	I_{cold}	I_{hot}	I_{low}	λ^a_{expt}	λ^b_{expt}	λ^c_{fit}	λ^d_{theo}	λ^e_{theo}
$C17$	FeXXI	$1s^22s^22p^2\ ^1D_2 - 1s2s^22p^3\ ^3D_3$	9.0	1.6	4.3	1.90173(40)		1.90195	1.90195	1.9009
$C18$	FeXXI	$1s^22s^22p^2\ ^1S_0 - 1s2s^22p^3\ ^3P_1$	1.8	0.3	0.6			1.90235	1.90235	1.9012
$N1$	FeXX	$1s^22s^22p^3\ ^2D_{3/2} - 1s2s^22p^4\ ^2P_{1/2}$	6.1	0.6	1.0	1.90286(40)		1.90295	1.90295	1.9020
$C19$	FeXXI	$1s^22s^22p^2\ ^1D_2 - 1s2s^22p^3\ ^3D_2$	1.4	0.3	2.1			1.90305	1.90305	1.9020
$N2$	FeXX	$1s^22s^22p^3\ ^2D_{5/2} - 1s2s^22p^4\ ^2P_{3/2}$	14.2	1.5	0.0	1.90361(40)		1.90370	1.90385	1.9028
$N3$	FeXX	$1s^22s^22p^3\ ^2P_{3/2} - 1s2s^22p^4\ ^2S_{1/2}$	13.0	1.3	5.2	⟨1.90463(40)⟩		1.90450	1.90435	1.9032
$N4$	FeXX	$1s^22s^22p^3\ ^4S_{3/2} - 1s2s^22p^4\ ^4P_{1/2}$	4.6	0.5	8.5	⟨1.90463(40)⟩		1.90495	1.90495	1.9037
$N5$	FeXX	$1s^22s^22p^3\ ^4S_{3/2} - 1s2s^22p^4\ ^2P_{3/2}$	9.9	1.0	35.1	⟨1.90463(40)⟩	1.90552(21)[f]	1.90520	1.90565	1.9043
$N6$	FeXX	$1s^22s^22p^3\ ^2D_{5/2} - 1s2s^22p^4\ ^2D_{5/2}$	19.6	2.0	1.6	⟨1.90555(40)⟩		1.90565	1.90595	1.9048
$N7$	FeXX	$1s^22s^22p^3\ ^2D_{3/2} - 1s2s^22p^4\ ^2D_{3/2}$	19.0	2.0	13.1	⟨1.90555(40)⟩		1.90605	1.90595	1.9049
$N8$	FeXX	$1s^22s^22p^3\ ^2P_{1/2} - 1s2s^22p^4\ ^2P_{3/2}$	5.4	0.6	1.6	⟨1.90690(40)⟩		1.90705	1.90705	1.9058
$N9$	FeXX	$1s^22s^22p^3\ ^2D_{5/2} - 1s2s^22p^4\ ^2D_{3/2}$	3.2	0.3	2.2	⟨1.90690(40)⟩		1.90725	1.90725	1.9062
$N10$	FeXX	$1s^22s^22p^3\ ^2P_{1/2} - 1s2s^22p^4\ ^2P_{1/2}$	6.3	0.7	1.1	⟨1.90690(40)⟩		1.90745	1.90745	1.9063
$N11$	FeXX	$1s^22s^22p^3\ ^4S_{3/2} - 1s2s^22p^4\ ^4P_{5/2}$	12.6	1.3	60.0	⟨1.90813(40)⟩	1.90829(14)	1.90845	1.90845	1.9072
$N12$	FeXX	$1s^22s^22p^3\ ^2P_{3/2} - 1s2s^22p^4\ ^2P_{3/2}$	4.9	0.5	1.5	⟨1.90813(40)⟩		1.90845	1.90925	1.9081
$N13$	FeXX	$1s^22s^22p^3\ ^2P_{3/2} - 1s2s^22p^4\ ^2P_{1/2}$	1.6	0.2	0.3			1.90960		1.9086

[a]present measurement; all wavelengths are determined relative to λ=1.85030 Å of line w.

[b]Seely, Feldman, and Safronova (1986); wavelengths are shifted by 0.16 mÅ in accordance with present choice of reference wavelength.

[c]values used in generating our synthetic spectra.

[d]semiempirical results from Z-expansion calculation of Seely, Feldman, and Safronova (1986).

[e]present calculation using the RAC code.

[f]identified as $N5$, but blends with $N7$.

TABLE VI. Line identification of features in the wavelength region 1.910 – 1.940 Å, which contains predominantly transitions from Fe XIX. I_{cold} and I_{hot} denote relative theoretical intensities for the plasma conditions shown in Fig. 1 calculated in the intermediate-density approximation. I_{low} denotes relative theoretical intensities for the "cold" plasma condition shown in Fig. 1 calculated in the low-density approximation. All wavelength values are in Ångstroms. Uncertainties in the measured wavelengths are in parentheses. ⟨⟩ denotes blends.

Label	Ion	Transition	I_{cold}	I_{hot}	I_{low}	λ^a_{expt}	λ^b_{expt}	λ^c_{fit}	λ^d_{theo}	λ^e_{theo}
$N14$	FeXX	$1s^22s^22p^3\ ^2P_{3/2} - 1s2s^22p^4\ ^2D_{5/2}$	9.1	0.9	0.8	1.91359(50)		1.91400	1.91125	1.9100
$N15$	FeXX	$1s^22s^22p^3\ ^2D_{5/2} - 1s2s^22p^4\ ^4P_{5/2}$	1.2	0.1	4.3			1.91460		1.9138
$O1$	FeXIX	$1s^22s^22p^4\ ^3P_2 - 1s2s^22p^5\ ^3P_1$	5.5	0.4	2.5	⟨1.91550(80)⟩		1.91545	1.91545	1.9139
$O2$	FeXIX	$1s^22s^22p^4\ ^1S_0 - 1s2s^22p^5\ ^1P_1$	3.4	0.2	0.0	⟨1.91550(80)⟩		1.91620		1.9145
$O3$	FeXIX	$1s^22s^22p^4\ ^1D_2 - 1s2s^22p^5\ ^1P_1$	14.3	1.0	0.4	⟨1.91550(80)⟩		1.91625	1.91625	1.9148
$O4$	FeXIX	$1s^22s^22p^4\ ^3P_2 - 1s2s^22p^5\ ^3P_2$	11.6	0.8	7.2	1.91700(50)	1.91749(44)	1.91765	1.91765	1.9160
$O5$	FeXIX	$1s^22s^22p^4\ ^3P_0 - 1s2s^22p^5\ ^3P_1$	3.4	0.2	0.3			1.91825	1.91825	1.9166
$O6$	FeXIX	$1s^22s^22p^4\ ^3P_1 - 1s2s^22p^5\ ^3P_1$	2.1	0.2	0.2			1.91875	1.91875	1.9171
$O7$	FeXIX	$1s^22s^22p^4\ ^3P_1 - 1s2s^22p^5\ ^3P_2$	4.3	0.3	0.5	1.92043(60)		1.92085	1.92085	1.9193
$O8$	FeXIX	$1s^22s^22p^4\ ^1D_2 - 1s2s^22p^5\ ^3P_1$	1.0	0.1	0.1			1.92160		1.9201
$O9$	FeXIX	$1s^22s^22p^4\ ^1S_0 - 1s2s^22p^5\ ^1P_1$	3.3	0.2	0.1	1.92310(60)		1.92300	1.92205	1.9203
$O10$	FeXIX	$1s^22s^22p^4\ ^1D_2 - 1s2s^22p^5\ ^3P_2$	1.3	0.1	0.2			1.92360		1.9223
$F1$	FeXVIII	$1s^22s^22p^5\ ^2P_{3/2} - 1s2s^22p^6\ ^2S_{1/2}$	6.2	0.4	3.1	1.92640(60)	1.92148(20)[f]	1.92755	1.92145	1.9254
$F2$	FeXVIII	$1s^22s^22p^5\ ^2P_{1/2} - 1s2s^22p^6\ ^2S_{1/2}$	3.1	0.2	0.5	1.93050(80)		1.93125	1.93125	1.9291

[a] present measurement; all wavelengths are determined relative to λ=1.85030 Å of line w.

[b] Seely, Feldman, and Safronova (1986); wavelengths are shifted by 0.16 mÅ in accordance with present choice of reference wavelength.

[c] values used in generating our synthetic spectra.

[d] semiempirical results from Z-expansion calculation of Seely, Feldman, and Safronova (1986).

[e] present calculation using the RAC code.

[f] possibly misidentified.

Figures

FIG. 1. Plasma conditions for the present measurements: (a) electron temperature profiles corresponding to the "hot" case (solid line) and "cold" case (dashed-line) referred to in the text. The profiles are inferred from electron cyclotron emission data and have been symmetrized for use as input in the modeling codes. The error bar indicates typical scatter in the data. (b) electron density profile measured with Thomson scattering. The density profiles for the "hot" and "cold" case are indistiguishable.

FIG. 2. Radial distribution of iron ions in PLT plasma. The profiles were computed with the MIST code for the "hot" plasma conditions given in Fig. 1. The calculations assume a radial diffusion coefficient of D=3000 cm^2/s.

FIG. 3. Schematic of the high-resolution, helium-filled spectrometer on the PLT tokamak. The spectrometer views the horizontal midplane of PLT. In accordance with Bragg's law, x rays of different wavelength λ are focussed at different positions along the position-sensitive detector. Displacements perpendicular to the line of sight are exaggerated for clarity.

FIG. 4. Kα spectra of iron for the "cold" plasma temperature case of Fig. 1: (a) Spectral emission observed on the PLT tokamak; a given spectral feature is labeled by the ionic species contributing most to its intensity. Lines from heliumlike Fe XXV are labeled individually in the notation of Gabriel (1972). (b) Synthetic iron Kα spectrum calculated from rates valid in the intermediate-density regime; the calculations use the the "cold" plasma parameters of Fig. 1 and assume a diffusion coefficient of D=3000 cm^2/s. (c) Synthetic iron Kα spectrum calculated from rates valid in the low-density limit; the assumed parameters are the same as in (b). The spectral resolving power is set to $\lambda/\Delta\lambda$=3000 in each synthetic spectrum for comparison with the observed emission in (a). Note that the emission of the heliumlike lines is not included in the model calculations.

FIG. 5. Kα spectra of iron for the "hot" plasma temperature case of Fig. 1: (a) Spectral emission observed on the PLT tokamak; a given spectral feature is labeled by the ionic species contributing most to its intensity. Lines from heliumlike Fe XXV are labeled individually in the notation of Gabriel (1972). (b) Synthetic iron Kα spectrum calculated from rates valid in the intermediate-density regime; the calculations use the "hot" plasma parameters of Fig. 1 and assume a diffusion coefficient of D=3000 cm^2/s. (c) Synthetic iron Kα spectrum calculated from rates valid in the low-density limit;

the assumed parameters are the same as in (b). The spectral resolving power is set to $\lambda/\Delta\lambda$=3000 in each synthetic spectrum for comparison with the observed emission in (a). Note that the emission of the heliumlike lines is not included in the model calculations.

FIG. 6. Synthetic iron Kα spectra generated with the model described in the text assuming coronal equilibrium and an electron temperature of 862 eV. The spectra include line emission from Fe XVIII through Fe XXIV, i.e., the line emission from Fe XXV is omitted. (a) charge balance calculated with ionization and recombination rates of Post *et al.* (1977) and line positions from Jacobs *et al.* (1989). (b) same as (a), except ionization rates are increased by $\times 1.4$. (c) same as (b), except line positions are those calculated by Seely, Feldman, and Safronova (1986), augmented and modified by our structure calculations. Spectral linewidth $\Delta\lambda=\lambda/3000$ is assumed to allow the summation of adjacent transitions.

FIG. 7. Iron Kα spectrum measured on the PLT tokamak. The data have been accumulated by integrating over 24 discharges and are plotted on a logarithmic scale to emphasize weak transitions. Features are labeled by the individual lines that contribute at least 20% of the intensity; a line contributing more than 50% of the total is underlined. Lowercase letters refer to heliumlike and lithiumlike transitions in the notation of Gabriel (1972). E denotes berylliumlike transitions, B boronlike transitions, C carbonlike transitions, N nitrogenlike transitions, O oxygenlike transitions, and F fluorinelike transitions.

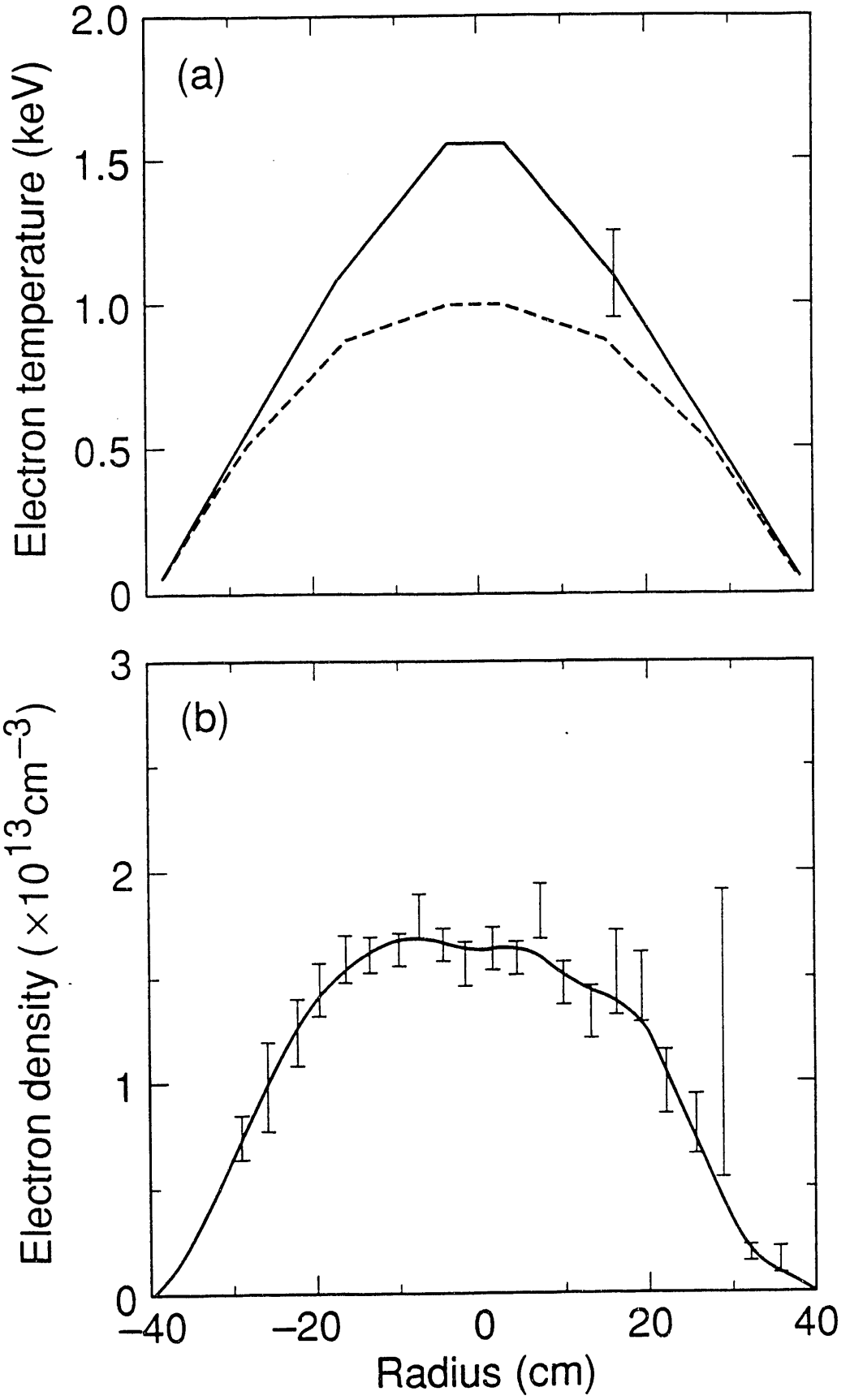

MX-042-U-15180/F 5

Figure 1.

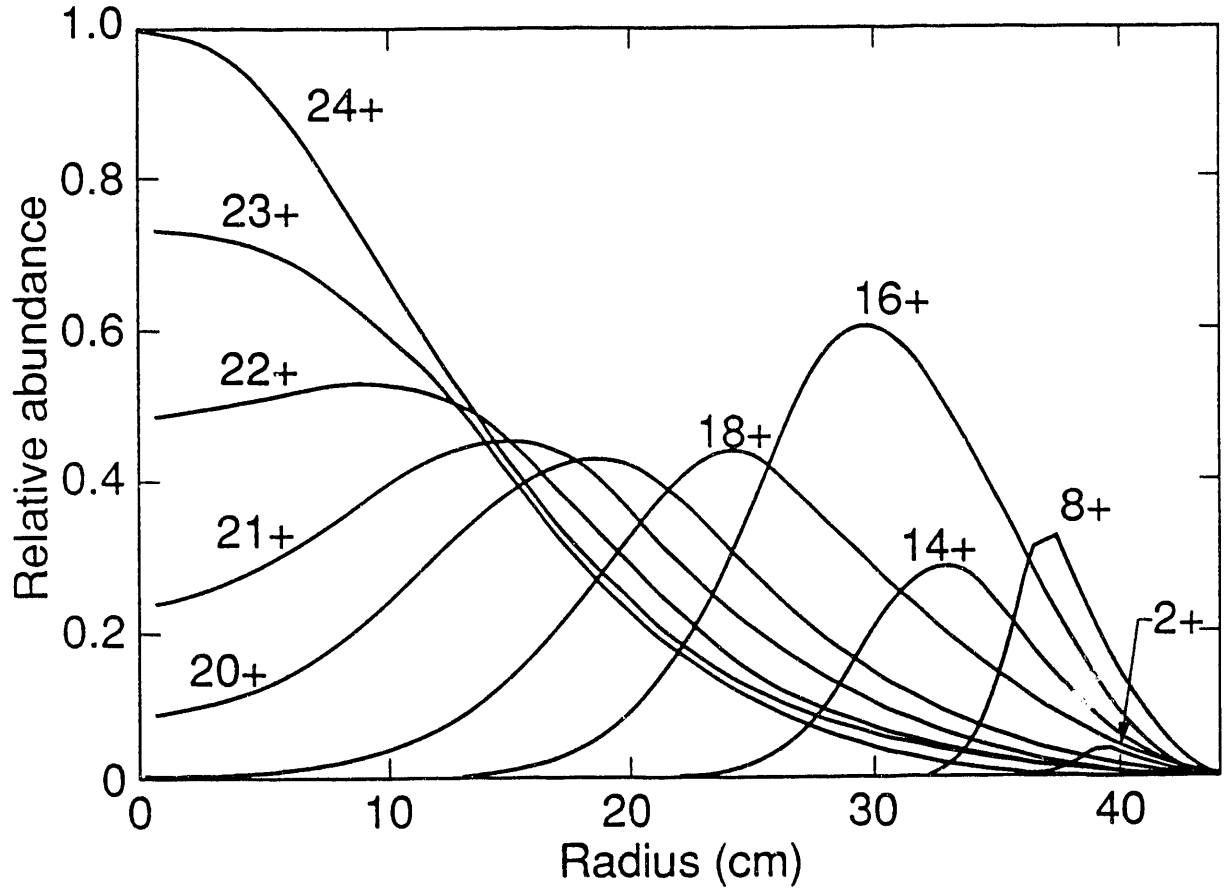

Figure 2.

QT-PeR-U-15608-01

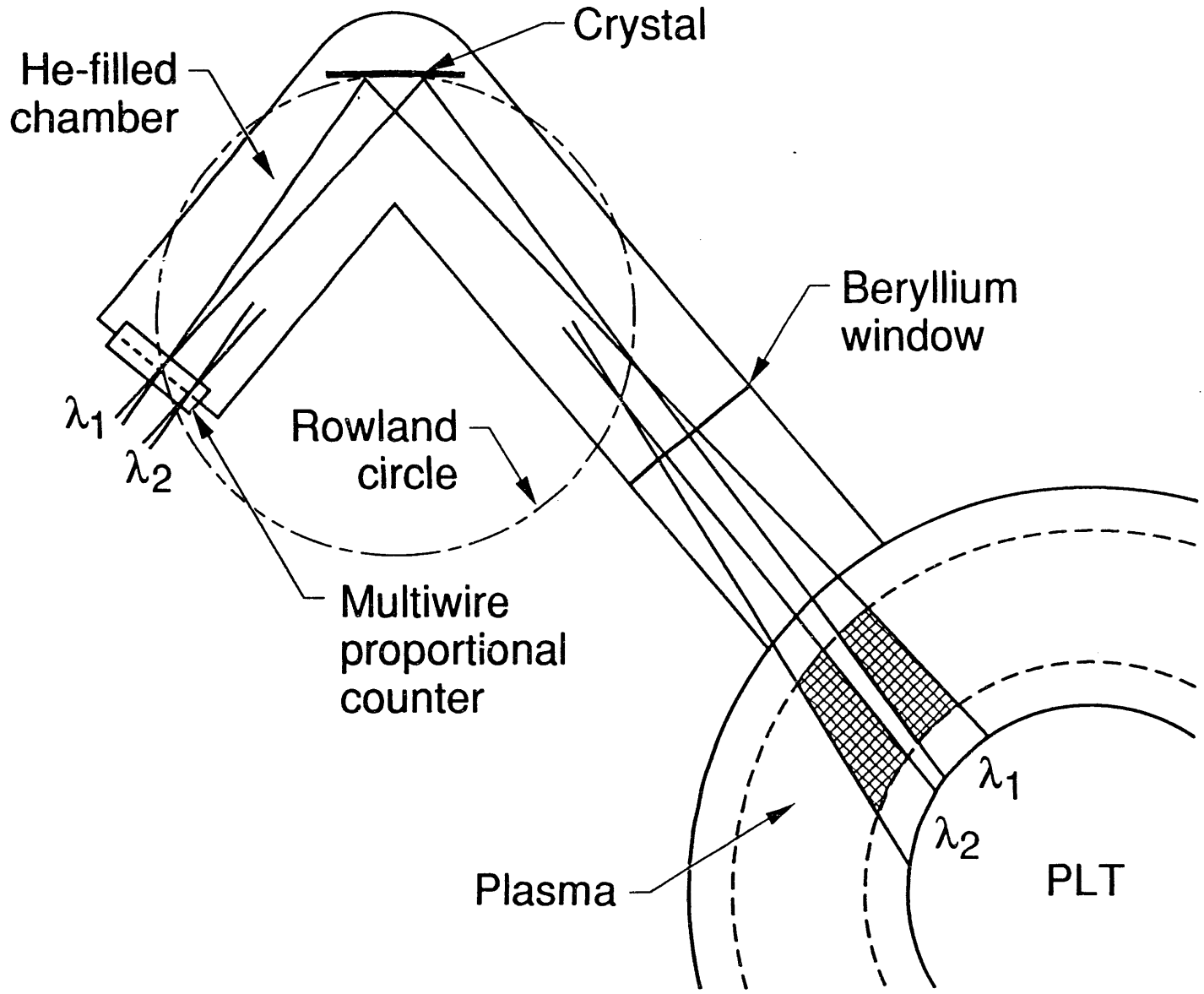

MX-042-U-15180/F 2

Figure 3.

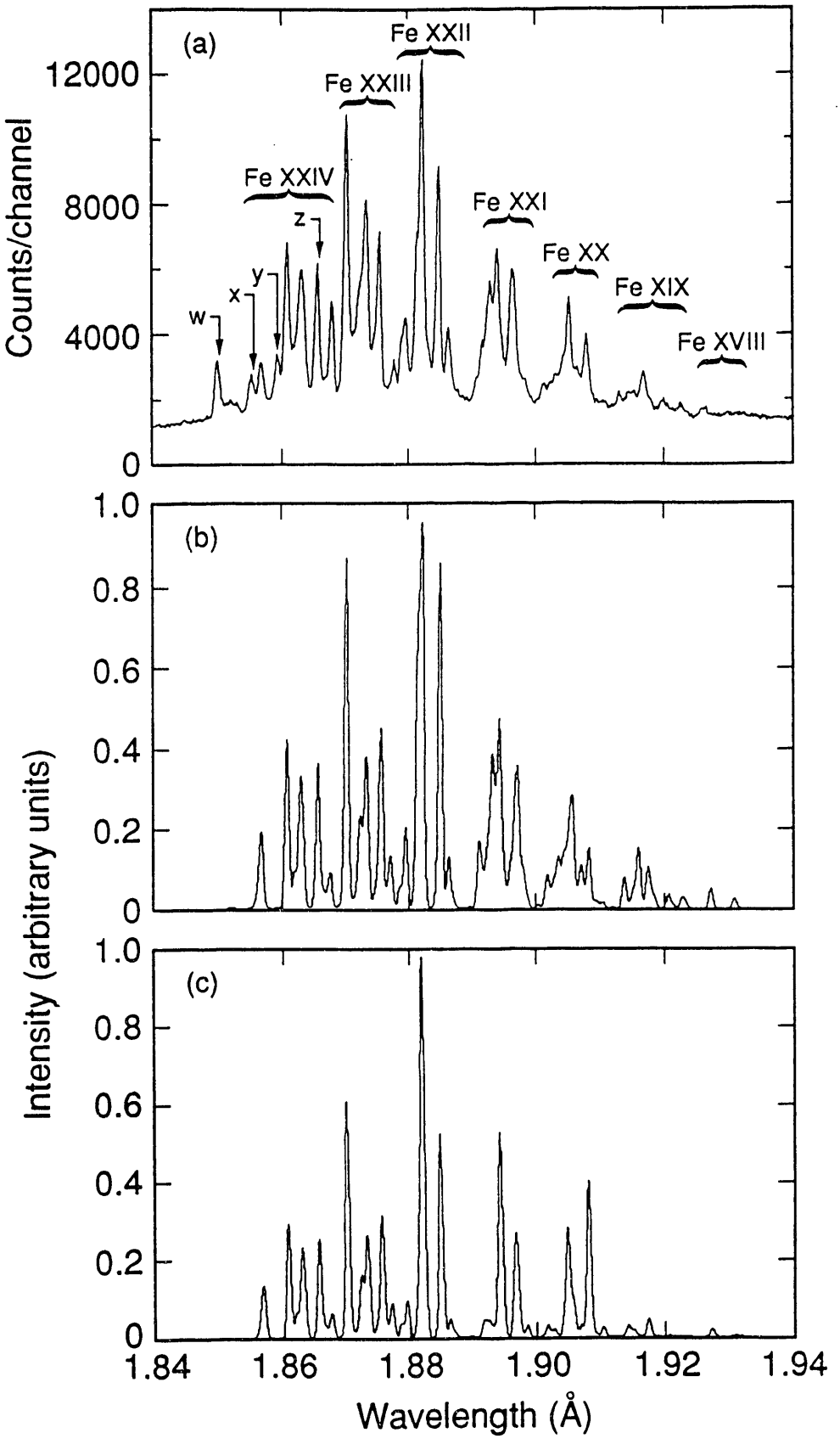

MX-056-U-22597/F 1

Figure 4.

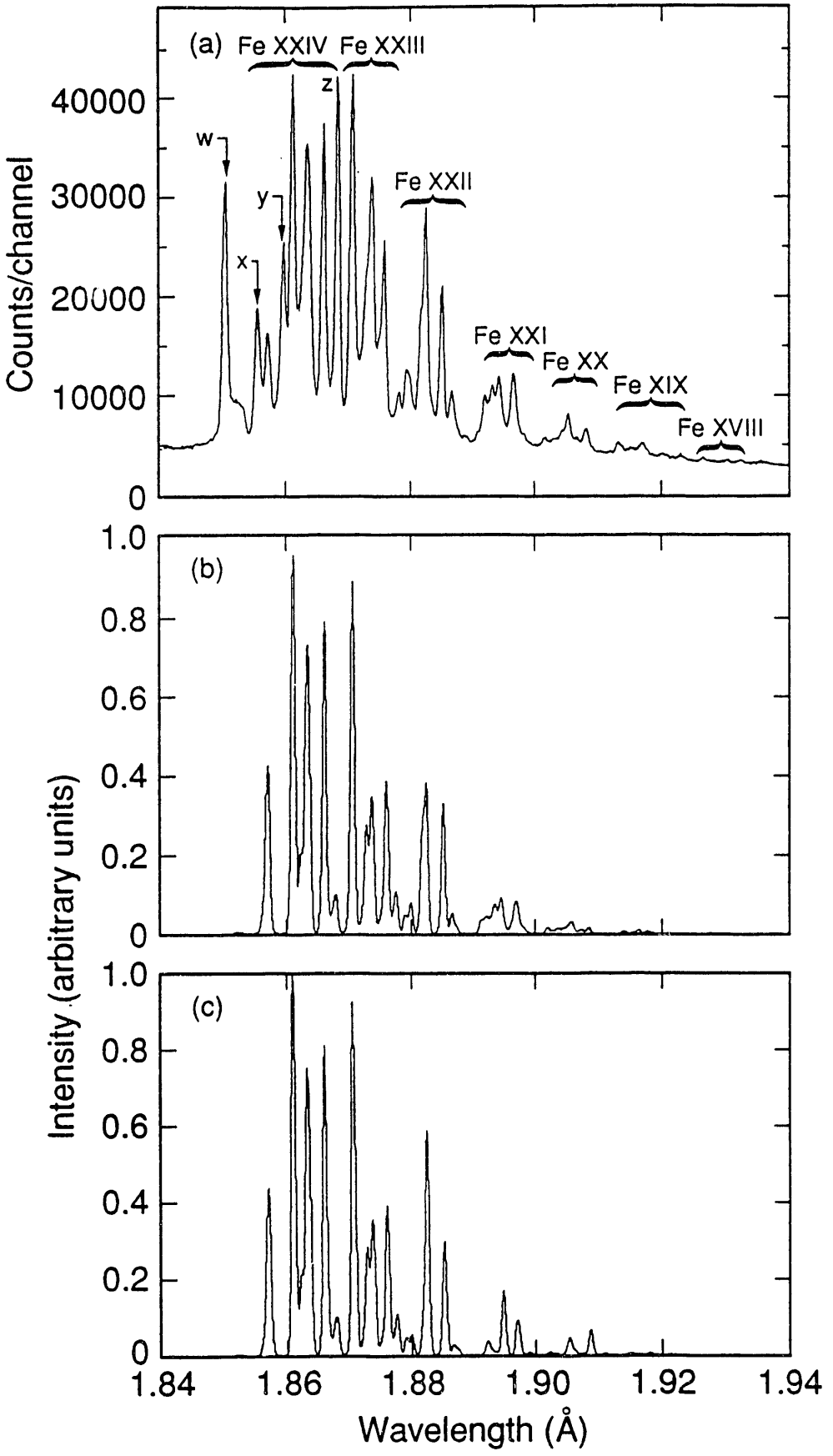

MX-056-U-22597/F 2

Figure 5.

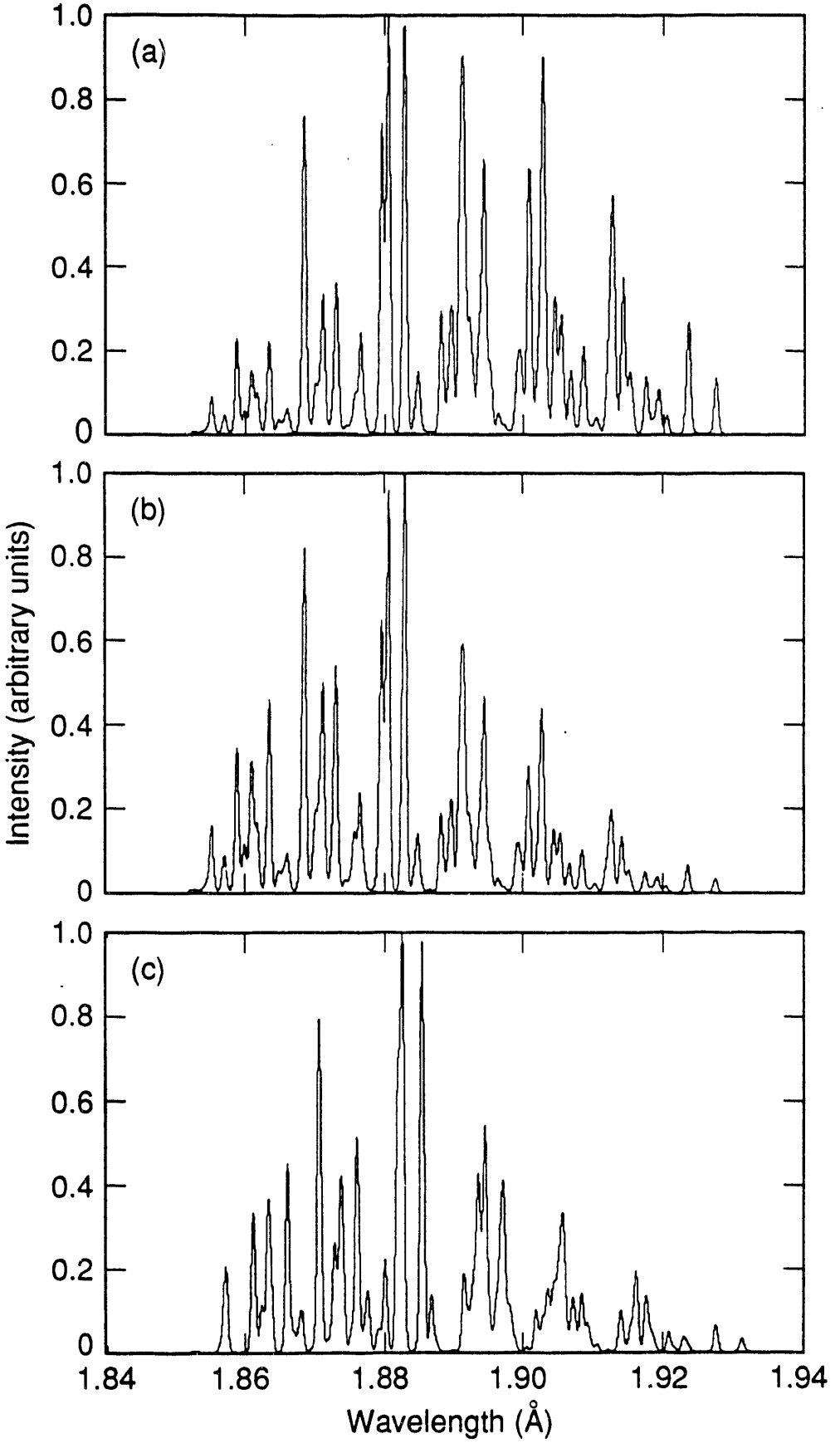

MX-050-U-19526/F 3

Figure 6.

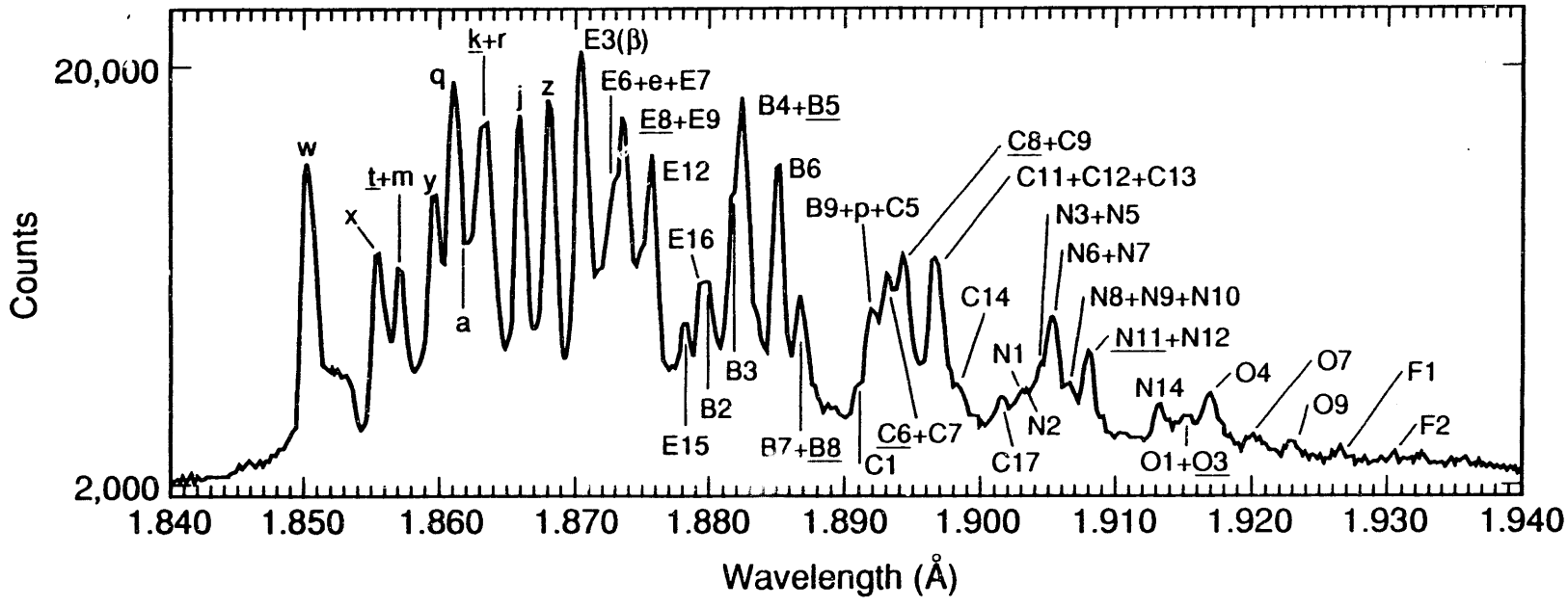

Figure 7.

MX-051-U-15608/F 1

EXTERNAL DISTRIBUTION IN ADDITION TO UC-420

Dr. F. Paoloni, Univ. of Wollongong, AUSTRALIA
Prof. M.H. Brennan, Univ. of Sydney, AUSTRALIA
Plasma Research Lab., Australian Nat. Univ., AUSTRALIA
Prof. I.R. Jones, Flinders Univ, AUSTRALIA
Prof. F. Cap, Inst. for Theoretical Physics, AUSTRIA
Prof. M. Heindler, Institut für Theoretische Physik, AUSTRIA
Prof. M. Goossens, Astronomisch Instituut, BELGIUM
Ecole Royale Militaire, Lab. de Phy. Plasmas, BELGIUM
Commission-European, DG. XII-Fusion Prog., BELGIUM
Prof. R. Boucique, Rijksuniversiteit Gent, BELGIUM
Dr. P.H. Sakanaka, Instituto Fisica, BRAZIL
Instituto Nacional De Pesquisas Especiais-INPE, BRAZIL
Documents Office, Atomic Energy of Canada Ltd., CANADA
Dr. M.P. Bachynski, MPB Technologies, Inc., CANADA
Dr. H.M. Skarsgard, Univ. of Saskatchewan, CANADA
Prof. J. Teichmann, Univ. of Montreal, CANADA
Prof. S.R. Sreenivasan, Univ. of Calgary, CANADA
Prof. T.W. Johnston, INRS-Energie, CANADA
Dr. R. Bolton, Centre canadien de fusion magnétique, CANADA
Dr. C.R. James,, Univ. of Alberta, CANADA
Dr. P. Lukác, Komenského Universzita, CZECHO-SLOVAKIA
The Librarian, Culham Laboratory, ENGLAND
Library, R61, Rutherford Appleton Laboratory, ENGLAND
Mrs. S.A. Hutchinson, JET Library, ENGLAND
Dr. S.C. Sharma, Univ. of South Pacific, FIJI ISLANDS
P. Mähönen, Univ. of Helsinki, FINLAND
Prof. M.N. Bussac, Ecole Polytechnique,, FRANCE
C. Mouttet, Lab. de Physique des Milieux Ionisés, FRANCE
J. Radet, CEN/CADARACHE - Bat 506, FRANCE
Prof. E. Economou, Univ. of Crete, GREECE
Ms. C. Rinni, Univ. of Ioannina, GREECE
Dr. T. Mual, Academy Bibliographic Ser., HONG KONG
Preprint Library, Hungarian Academy of Sci., HUNGARY
Dr. B. DasGupta, Saha Inst. of Nuclear Physics, INDIA
Dr. P. Kaw, Inst. for Plasma Research, INDIA
Dr. P. Rosenau, Israel Inst. of Technology, ISRAEL
Librarian, International Center for Theo Physics, ITALY
Miss C. De Palo, Associazione EURATOM-ENEA , ITALY
Dr. G. Grosso, Istituto di Fisica del Plasma, ITALY
Prof. G. Rostangni, Istituto Gas Ionizzati Del Cnr, ITALY
Dr. H. Yamato, Toshiba Res & Devel Center, JAPAN
Prof. I. Kawakami, Hiroshima Univ., JAPAN
Prof. K. Nishikawa, Hiroshima Univ., JAPAN
Director, Japan Atomic Energy Research Inst., JAPAN
Prof. S. Itoh, Kyushu Univ., JAPAN
Research Info. Ctr., National Instit. for Fusion Science, JAPAN
Prof. S. Tanaka, Kyoto Univ., JAPAN
Library, Kyoto Univ., JAPAN
Prof. N. Inoue, Univ. of Tokyo, JAPAN
Secretary, Plasma Section, Electrotechnical Lab., JAPAN
S. Mori, Technical Advisor, JAERI, JAPAN
Dr. O. Mitarai, Kumamoto Inst. of Technology, JAPAN
J. Hyeon-Sook, Korea Atomic Energy Research Inst., KOREA
D.I. Choi, The Korea Adv. Inst. of Sci. & Tech., KOREA
Prof. B.S. Liley, Univ. of Waikato, NEW ZEALAND
Inst of Physics Chinese Acad Sci PEOPLE'S REP. OF CHINA
Library, Inst. of Plasma Physics, PEOPLE'S REP. OF CHINA
Tsinghua Univ. Library, PEOPLE'S REPUBLIC OF CHINA
Z. Li, S.W. Inst Physics, PEOPLE'S REPUBLIC OF CHINA
Prof. J.A.C. Cabral, Instituto Superior Tecnico, PORTUGAL
Dr. O. Petrus, AL I CUZA Univ , ROMANIA
Dr. J. de Villiers, Fusion Studies, AEC, S. AFRICA
Prof. M.A. Hellberg, Univ. of Natal, S. AFRICA
Prof. D.E. Kim, Pohang Inst. of Sci. & Tech., SO. KOREA
Prof. C.I.E.M.A.T, Fusion Division Library, SPAIN
Dr. L. Stenflo, Univ. of UMEA, SWEDEN
Library, Royal Inst. of Technology, SWEDEN
Prof. H. Wilhelmson, Chalmers Univ. of Tech., SWEDEN
Centre Phys. Des Plasmas, Ecole Polytech, SWITZERLAND
Bibliotheek, Inst. Voor Plasma-Fysica, THE NETHERLANDS
Asst. Prof. Dr. S. Cakir, Middle East Tech. Univ., TURKEY
Dr. V.A. Glukhikh,Sci. Res. Inst. Electrophys.I Apparatus, USSR
Dr. D.D. Ryutov, Siberian Branch of Academy of Sci., USSR
Dr. G.A. Eliseev, I.V. Kurchatov Inst., USSR
Librarian, The Ukr.SSR Academy of Sciences, USSR
Dr. L.M. Kovrizhnykh, Inst. of General Physics, USSR
Kernforschungsanlage GmbH, Zentralbibliothek, W. GERMANY
Bibliothek, Inst. Für Plasmaforschung, W. GERMANY
Prof. K. Schindler, Ruhr-Universität Bochum, W. GERMANY
Dr. F. Wagner, (ASDEX), Max-Planck-Institut, W. GERMANY
Librarian, Max-Planck-Institut, W. GERMANY
Prof. R.K. Janev, Inst. of Physics, YUGOSLAVIA

END

DATE
FILMED
3/9/93